HAL
open science

Tracing water masses with 129I and 236U in the subpolar North Atlantic along the GEOTRACES GA01 section

Maxi Castrillejo, Núria Casacuberta, Marcus Christl, Christof Vockenhuber, Hans-Arno Synal, Maribel I. García-Ibáñeza, Pascale Lherminier, Géraldine Sarthou, Jordi Garcia-Orellanac, Pere Masqué

To cite this version:

Maxi Castrillejo, Núria Casacuberta, Marcus Christl, Christof Vockenhuber, Hans-Arno Synal, et al.. Tracing water masses with 129I and 236U in the subpolar North Atlantic along the GEOTRACES GA01 section. Biogeosciences, 2018, 15 (18), pp.5545-5564. 10.5194/bg-15-5545-2018 . hal-02322755

HAL Id: hal-02322755

https://hal.science/hal-02322755

Submitted on 21 May 2020

HAL is a multi-disciplinary open access archive for the deposit and dissemination of scientific research documents, whether they are published or not. The documents may come from teaching and research institutions in France or abroad, or from public or private research centers.

L'archive ouverte pluridisciplinaire **HAL**, est destinée au dépôt et à la diffusion de documents scientifiques de niveau recherche, publiés ou non, émanant des établissements d'enseignement et de recherche français ou étrangers, des laboratoires publics ou privés.

Biogeosciences, 15, 5545–5564, 2018
https://doi.org/10.5194/bg-15-5545-2018
© Author(s) 2018. This work is distributed under
the Creative Commons Attribution 4.0 License.

Biogeosciences
Open Access

Tracing water masses with ^{129}I and ^{236}U in the subpolar North Atlantic along the GEOTRACES GA01 section

Maxi Castrillejo[1,2], Núria Casacuberta[1,3], Marcus Christl[1], Christof Vockenhuber[1], Hans-Arno Synal[1], Maribel I. García-Ibáñez[4,5], Pascale Lherminier[6], Géraldine Sarthou[7], Jordi Garcia-Orellana[2,8], and Pere Masqué[2,8,9]

[1]Laboratory of Ion Beam Physics, ETH Zurich, Otto Stern Weg 5, Zurich, 8093, Switzerland
[2]Institut de Ciència i Tecnologia Ambientals, Universitat Autònoma de Barcelona, Bellaterra, 08193, Spain
[3]Institute of Biogeochemistry and Pollutant Dynamics, Environmental Physics, ETH Zurich, Universitätstrasse 16, Zurich, 8092, Switzerland
[4]Uni Research Climate, Bjerknes Centre for Climate Research, Bergen 5008, Norway
[5]Instituto de Investigaciones Marinas (IIM-CSIC), Eduardo Cabello 6, 36208 Vigo, Spain
[6]Ifremer, Univ. Brest, CNRS, IRD, Laboratoire d' Océanographie Physique et Spatiale, IUEM, Plouzané, France
[7]Laboratoire des Sciences de l'Environnement Marin (LEMAR), UMR 6539 CNRS UBO IRD Ifremer, IUEM, Technopôle Brest Iroise, 29280 Plouzané, France
[8]Departament de Fisica, Universitat Autònoma de Barcelona, Bellaterra, 08193, Spain
[9]School of Science, Centre for Marine Ecosystems Research, Edith Cowan University, Joondalup, WA 6027, Australia

Correspondence: Maxi Castrillejo (maxic@phys.ethz.ch)

Received: 11 May 2018 – Discussion started: 25 May 2018
Revised: 24 August 2018 – Accepted: 29 August 2018 – Published: 18 September 2018

Abstract. Pathways and timescales of water mass transport in the subpolar North Atlantic Ocean (SPNA) have been investigated by many studies due to their importance for the meridional overturning circulation and thus for the global ocean. In this sense, observational data on geochemical tracers provide complementary information to improve the current understanding of the circulation in the SPNA. To this end, we present the first simultaneous distribution of artificial ^{129}I and ^{236}U in 14 depth profiles and in surface waters along the GEOVIDE section covering a zonal transect through the SPNA in spring 2014. Our results show that the two tracers are distributed following the water mass structure and that their presence is largely influenced by the global fallout (GF) and liquid effluents discharged to north-western European coastal waters by the Sellafield and La Hague nuclear reprocessing plants (NRPs). As a result, ^{129}I concentrations and ^{236}U/^{238}U atom ratios and ^{129}I/^{236}U atom ratios display a wide range of values: (0.2–256) $\times 10^{7}$ at kg^{-1} (40–2350) $\times 10^{-12}$ and 0.5–200, respectively. The signal from NRPs, which is characterised by higher ^{129}I concentrations and ^{129}I/^{236}U atom ratios compared to GF, is transported by Atlantic Waters (AWs) into the SPNA, notably by the East Greenland Current (EGC)/Labrador Current (LC) at the surface and by waters overflowing the Greenland–Scotland passage at greater depths. Nevertheless, our results show that the effluents from NRPs may also directly enter the surface of the eastern SPNA through the Iceland–Scotland passage or the English Channel/Irish Sea. The use of the ^{236}U/^{238}U and ^{129}I/^{236}U dual tracer approach further serves to discern Polar Intermediate Water (PIW) of Canadian origin from that of Atlantic origin, which carries comparably higher tracer levels due to NRPs (particularly ^{129}I). The cascading of these waters appears to modify the water mass composition in the bottom of the Irminger and Labrador seas, which are dominated by Denmark Strait Overflow Water (DSOW). Indeed, PIW–Atlantic, which has a high level of ^{129}I compared to ^{236}U, appears to contribute to the deep Irminger Sea increasing the ^{129}I concentrations in the realm of DSOW. A similar observation can be made for ^{236}U for PIW entering through the Canadian Archipelago into the Labrador Sea. Several depth profiles also show an increase in ^{129}I concentrations in near bottom waters in the Iceland and the West European basins that are very likely associated with the transport of the NRP signal by the Iceland–Scotland Overflow Wa-

ter (ISOW). This novel result would support current modelling studies indicating the transport of ISOW into the eastern SPNA. Finally, our tracer data from 2014 are combined with published ^{129}I data for the deep central Labrador Sea between 1993 and 2013. The results obtained from comparing simulated and measured ^{129}I concentrations support the previously suggested two major transport pathways for the AWs in the SPNA, i.e. a short loop through the Nordic seas into the SPNA and a longer loop, which includes recirculation of the AWs in the Arctic Ocean before it enters the western SPNA.

1 Introduction

The subpolar North Atlantic (SPNA) is a key region for the global ocean circulation (see all acronyms in the Appendix). The North Atlantic Current (NAC) carries warm subtropical waters northwards to the SPNA, where they are transformed into cold Subpolar Mode Water (SPMW) and ultimately into Labrador Sea Water (LSW), which circulates southwards along with the overflow waters from the Nordic seas (Fig. 1). These water mass formation processes constitute the starting point of the Atlantic meridional overturning circulation (AMOC). Among other studies, the repeated hydrographic cruises along the Greenland–Portugal OVIDE line shed light on the decadal variability of the AMOC (Daniault et al., 2016; Lherminier et al., 2010; Mercier et al., 2013) and its relevance to climate, for example, by controlling the ocean uptake of CO_2 (Pérez et al., 2013). The GEOVIDE cruise carried out in spring 2014 covered the OVIDE line, extending further to the Labrador Sea and revealing an intense AMOC over a cold and fresh SPNA (Zunino et al., 2017). The observed strong AMOC was linked to an intensified poleward transport of subtropical waters as well as to the increased equatorward transport of Iceland–Scotland Overflow Water (ISOW), Irminger–SPMW (IrSPMW) and Polar Intermediate Water (PIW) in 2014 relative to mean 2002–2010 (García-Ibáñez et al., 2018).

Anthropogenic tracers provide complementary information about the above-water mass circulation changes in the SPNA. For example, chlorofluorocarbons (CFCs) and sulfur hexafluoride (SF_6) from industrial activities or tritium (^{3}H) from atmospheric nuclear weapon tests conducted in the 1950s and 1960s (global fallout, GF) provide information on the ventilation of the interior Atlantic Ocean (Doney and Jenkins, 1994; Sy et al., 1997; Tanhua et al., 2005). Contrary to CFCs or ^{3}H, which were introduced into the surface ocean from a rather well-mixed atmosphere, nuclear reprocessing plants (NRPs) represent point-like sources of artificial radionuclides. The NRPs located near La Hague and Sellafield discharge(d) liquid effluents to the English Channel and the Irish Sea, respectively, over the past 50–60 years, thereby tagging Atlantic waters (AWs) passing these locations from the 1960s on (Kershaw and Baxter, 1995). This allowed an investigation of AW-spreading pathways and timescales downstream of these nuclear facilities (e.g. Aarkrog et al., 1983, 1987, Alfimov et al., 2004, 2013; Beasley et al., 1998; Casacuberta et al., 2016, 2018; Christl et al., 2015b; Dahlgaard, 1995; Edmonds et al., 2001; Holm et al., 1983; Smith et al., 1998, 2005, 2011, 2016). The schematic transport of NRP effluents and water masses in the SPNA–Arctic Ocean region is displayed in Fig. 1. NRP-labelled AWs are first transported by surface currents into the North Sea and then carried poleward by the Norwegian Coastal Current (NCC) into the Nordic seas (Edmonds et al., 1998; Raisbeck and Yiou, 2002) while mixing with the Norwegian Atlantic Current (NwAC) (Gascard et al., 2004; Kershaw and Baxter, 1995). The current splits in two branches north of Norway, one branch entering the Barents Sea as Barents Sea Branch Water (BSBW) and the other branch approaching the Fram Strait west of Spitsbergen, where it bifurcates again. One branch joins the East Greenland Current (EGC) and recirculates southwards as Return Atlantic Water (RAW) (Fogelqvist et al., 2003) mixing with IrSPMW and PIW (modified AW that has recirculated in the Arctic Ocean; Rudels et al., 1999b). The other branch, the West Spitsbergen Current (WSC), transports the remaining AWs at shallow to intermediate depths into the Arctic Ocean via the Fram Strait Branch Water (FSBW), where they recirculate in the Arctic Eurasian Basin before outflowing back through the Fram Strait and continuing southwards carried by the EGC (Rudels, 2015). The NRP signal also penetrates deep into the water column due to the formation of dense water north of the Greenland–Iceland and Iceland–Scotland passages, providing means of tracing the deep overflows that ventilate the deep North Atlantic Ocean (e.g. Smith et al., 2005). Thus, radionuclides discharged from European NRPs are particularly well suited to studying the water mass circulation in the SPNA (Fig. 1).

Among the set of radionuclides discharged from NRPs, the ^{129}I is regarded as a robust circulation tracer for investigating water mass transport pathways, advection and mixing, and for testing the performance of ocean circulation models in the Nordic seas, the Arctic Ocean and the Atlantic Ocean (Karcher et al., 2012; Orre et al., 2010; Smith et al., 2016). Firstly, ^{129}I can be detected at all oceanic levels far from the source thanks to its conservative behaviour in seawater, its long half-life ($T_{1/2} = 15.7$ Ma) and the low detection limits obtained with accelerator mass spectrometry (AMS) (e.g. Vockenhuber et al., 2015). Secondly, the presence of ^{129}I in those regions is dominated by the liquid discharge from European NRPs, which has a well-documented release history (> 5700 kg; He et al., 2013a; Raisbeck et al., 1995), while the contribution from GF is comparably negligible (> 90 kg worldwide release; Hou, 2004; Raisbeck and Yiou, 1999; Wagner et al., 1996). Consequently, the seawater affected by NRPs may present ^{129}I concentrations 1–4 orders of magnitude above the background due to GF ($\sim 2.5 \times 10^7$ at kg^{-1}; Edmonds et al., 1998). In the western SPNA, most of the ^{129}I is now present in the EGC, flowing across the Greenland

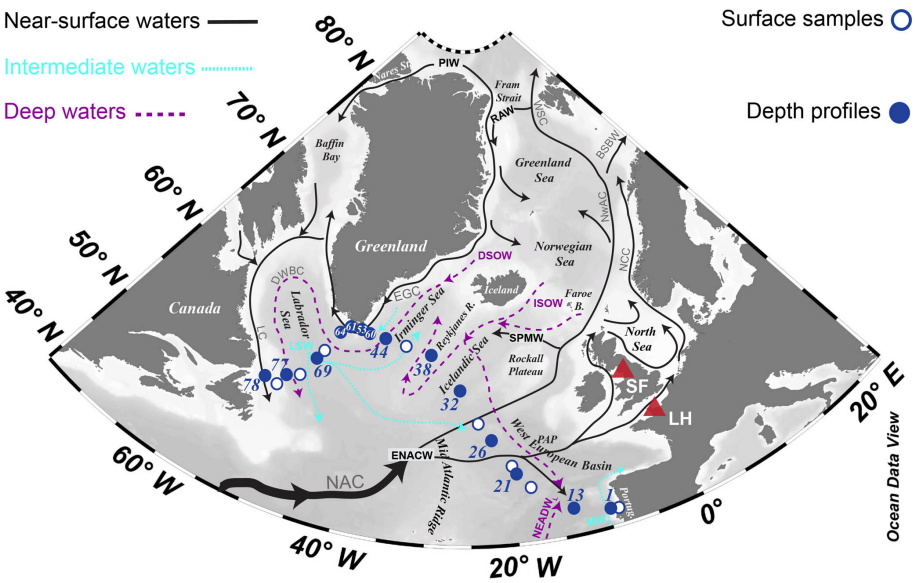

Figure 1. Sampled locations in the subpolar North Atlantic during the GEOVIDE cruise in spring 2014. The nuclear fuel reprocessing plants of La Hague (LH) and Sellafield (SF) are represented along with the main water masses and their schematic spreading pathways are adapted from Daniault et al. (2016) and Smith et al. (2005). Acronyms are defined in the Appendix.

Shelf (Alfimov et al., 2013) and in the Denmark Strait Overflow Water (DSOW) that fills bottom depths of the Irminger and Labrador seas (Smith et al., 2005, 2016). The other overflow water, ISOW, enters the North Atlantic through the Iceland–Scotland sill (Hansen and Osterhus, 2000) and is present notably along the Reykjanes Ridge or overlying DSOW in the Irminger and Labrador seas. ISOW carries comparably less ^{129}I (Edmonds et al., 2001), yet its ^{129}I concentrations at the sill have increased 900 % over the last 20 years (Alfimov et al., 2013; Edmonds et al., 2001; Vivo-Vilches et al., 2018), implying that this tracer may also provide a chronological marker for spreading pathways of overflow water in the eastern SPNA.

Uranium-236 ($T_{1/2} = 23.5$ Ma) is a long-lived conservative radionuclide similar to ^{129}I and a novel ocean circulation tracer investigated in the last decade (e.g. Casacuberta et al., 2014, 2016, 2018; Castrillejo et al., 2017; Christl et al., 2012; Christl et al., 2017; Sakaguchi et al., 2012; Winkler et al., 2012). Surface seawater in the Northern Hemisphere presents ^{236}U/^{238}U atom ratios of about 1000×10^{-12} (e.g. Christl et al., 2012) in the unique presence of GF (about 900 kg released worldwide; Sakaguchi et al., 2009). However, the ^{236}U/^{238}U ratios can be significantly higher in the Arctic and North Atlantic Oceans due to the liquid discharge of ^{236}U from European NRPs (about 100 kg, Christl et al., 2015a). This made it possible to trace the waters carrying NRP-^{236}U with ^{236}U/^{238}U ratios up to 3800×10^{-12} in the Arctic Ocean in 2011–2012 (Casacuberta et al., 2016) and up to 1400×10^{-12} in LSW and DSOW in the western SPNA in 2010 (Casacuberta et al., 2014). In addition, both ^{236}U and ^{129}I can be combined to form the dual tracer, ^{129}I/^{236}U–^{236}U/^{238}U, to identify the radionuclide source(s) present in a given water mass (Casacuberta et al., 2016; Christl et al., 2015b). This is possible because the GF and the European NRPs introduced different amounts of ^{236}U and ^{129}I (see above) into the environment and tagged the waters with characteristic ^{129}I/^{236}U and ^{236}U/^{238}U atom ratios depending on the proximity from the source(s). Consequently, this dual tracer could also help to better understand the mixing in the SPNA between AWs tagged by European NRPs and water masses carrying mainly GF (e.g. Arctic–Canadian water).

In this study, we aim to use artificial ^{129}I and ^{236}U to investigate the transport pathways and timescales of water mass circulation in the SPNA. To this end, we present the first simultaneous distribution of ^{129}I and ^{236}U along the GEOVIDE cruise track in spring 2014 (Fig. 1). The study pursues three specific objectives. Firstly, we study the zonal distribution of ^{129}I and ^{236}U and their relationship with the water mass structure. Although the distribution of ^{129}I in the Irminger and Labrador seas has been well studied in the last 30 years, there is a significant data gap east of the Reykjanes Ridge for ^{129}I and for most of the section for ^{236}U. Secondly, we use the dual ^{129}I/^{236}U–^{236}U/^{238}U tracer approach to distinguish the source contribution to the presence of ^{129}I and ^{236}U in the SPNA. This information is then valuable for studying the origin, mixing and spreading pathways of water masses participating in the AMOC. The combined use of ^{129}I and ^{236}U allows circulation features to be traced that received significant attention in earlier modelling, tracer and physical studies and helps to validate recent interpretations on the ventilation of the North Atlantic by overflow waters. Thirdly, tracer data from 2014 are combined with the exten-

sive ^{129}I time series in the central Labrador Sea to further investigate the circulation timescales of AWs downstream of European NRPs.

2 Materials and methods

2.1 The cruise, study area and sample collection

The GEOVIDE cruise (Fig. 1) covered the OVIDE line from Lisbon (Portugal) to the southern tip of Greenland (Cape Farewell), and from Cape Farewell to St John's (Newfoundland, Canada) on board the French R/V *Pourquoi pas?* between 15 May and 30 June 2014. This cruise is part of the GEOTRACES programme (section GA01: http://www.geotraces.org/cruises/cruise-summary, last acces: September 2018) and contributes to the decade-long biannual sampling (2002 to 2018) of the OVIDE line (http://www.umr-lops.fr/Projets/Projets-actifs/OVIDE, last acces: September 2018) from a geochemical perspective.

This study is based on concentrations of ^{129}I and ^{236}U, and on ^{236}U/^{238}U ratios determined in about 150 seawater samples collected from 14 depth profiles (Fig. 1) using a rosette equipped with conductivity–temperature–depth sensors and 24 Niskin bottles of 12 L each. To collect water, sampling depths were chosen from the main water masses and circulation features at each station by considering conductivity, temperature and oxygen profiles. From east to west (Fig. 1), depth profiles were located in the West European Basin (WEB: stations 1, 13, 21 and 26), the central Icelandic Basin (station 32), above the Reykjanes Ridge (station 38), the Irminger Sea (stations 44 and 60), the Labrador Sea (stations 64, 69 and 77), and on the shelf/slope of Greenland (stations 53 and 61) and Canada (station 78). Additional surface samples were obtained using a FISH device that allowed the collection of seawater from about 2 m depth at eight locations placed between depth profiles. Samples for ^{129}I of ~ 0.5 L were collected in dark plastic bottles and sealed with parafilm. The ^{236}U samples of 5–7 L were collected in plastic cubitainers. Bottles and cubitainers were rinsed 3 times with seawater before sample collection to avoid potential contamination.

2.2 Iodine-129 purification and AMS measurement

The radiochemistry of ^{129}I followed a method described in Michel et al. (2012) at EAWAG (Switzerland). About 300–450 mL of sample was spiked with ~ 1.5 mg of Woodward stable iodine (^{127}I) carrier. All iodine was oxidised to iodate by adding 2 % $Ca(ClO)_2$, then reduced to iodide using $Na_2S_2O_5$ and 1 M $NH_3O{\cdot}HCl$. The purification of iodine was carried out using columns filled with DOWEX® 1×8 ion exchange resin. The column was conditioned with deionised water and diluted KNO_3 solution before the elution of iodine with 2.25 M KNO_3 solution. The iodine was precipitated as AgI by adding $AgNO_3$, then mixed with 4–5 mg of Ag and pressed into AMS cathodes. The compact 0.5 MV Tandy AMS system at ETH Zurich was used to measure the ^{129}I/^{127}I atom ratios (Vockenhuber et al., 2015). The ^{129}I/^{127}I ratios were normalised with the ETH Zurich in-house standard D22 with a nominal ^{129}I/^{127}I value of $(50.35 \pm 0.16) \times 10^{-12}$ (Christl et al., 2013b). Radiochemistry blanks ($n = 24$) were prepared with deionised water and processed together with seawater samples following the same analytical procedures. These blanks presented ^{129}I/^{127}I ratios of $(0.7–4) \times 10^{-13}$ corresponding to $(0.5–3) \times 10^{6}$ atoms of ^{129}I. The ^{129}I concentrations were calculated based on measured ^{129}I/^{127}I ratio and the known amounts of ^{127}I carrier added to each sample. The detection limit of < 0.3 fg ^{129}I depended on the measured ^{129}I/^{127}I ratio of the Woodward iodine carrier, which is typically of the order of $\sim 10^{-13}$.

2.3 Uranium-236 purification and AMS measurement

Each seawater sample (5–7 L) was weighed, acidified to pH below 2 using concentrated suprapure HNO_3 and spiked with ~ 3 pg of ^{233}U (IRMM – 051). The uranium was co-precipitated with iron hydroxides upon addition of ~ 200 mg of U-free Fe^{2+} solution and concentrated suprapure NH_4OH by raising the pH to ~ 8. The iron precipitate was syphoned, evaporated to dryness and re-dissolved using 8 M HNO_3. The purification of uranium was carried out using UTEVA columns (Triskem). The eluate was co-precipitated with $\sim$ 1 mg of the U-free Fe^{2+} solution and evaporated to dryness. All uranium was converted to oxide form by heating the iron precipitates to 650 °C, then mixing them with 2–3 mg of niobium and pressing them into AMS cathodes. The compact 0.5 MV Tandy AMS system at ETH Zurich was used to measure ^{233}U, ^{236}U and ^{238}U following Christl et al. (2013a). The measured ^{236}U/^{233}U and ^{236}U/^{238}U ratios were normalised to the ZUTRI ETH Zurich in-house standard with nominal values of $(4055 \pm 200) \times 10^{-12}$ and $(33\,170 \pm 830) \times 10^{-12}$ (Christl et al., 2013a). Radiochemistry blanks ($n = 19$) were prepared on board and in the land-based laboratory with deionised water and processed together with seawater samples following same analytical procedures. The blanks presented ^{236}U/^{233}U ratios $< 10^{-4}$, corresponding to < 40 ag of ^{236}U. The compact TANDY AMS system has an abundance mass sensitivity of $\sim 10^{-12}$ for the mass range of actinides, corresponding to an estimated instrumental background level of the order of ^{236}U/^{238}U $\sim 10^{-14}$. Due to a mistake in the laboratory, a total of 34 samples were accidentally cross-contaminated with a very high ^{236}U standard and therefore had to be background corrected for cross talk. The uncertainty of this additional background correction led to higher errors reported for those samples (marked with an asterisk in Table 1).

Table 1. Concentrations of ^{129}I and ^{236}U, and atom ratios of ^{236}U/^{238}U and ^{129}I/^{236}U in seawater samples collected during the GEOVIDE cruise in spring 2014. Uncertainties of radionuclide concentrations and the ^{236}U/^{238}U ratio are given as 1σ deviations. The uncertainty of the ^{129}I/^{236}U ratio was propagated from the concentration uncertainty. * ^{236}U data are corrected for cross talk contamination. Temp. stands for temperature.

Station and location	ETH code	Depth m	Dominant water mass	Salinity	Potential temp. °C	Oxygen µmol kg^{-1}	^{129}I $\times 10^7$ at kg^{-1}	^{236}U $\times 10^6$ at kg^{-1}	^{236}U/^{238}U $\times 10^{-12}$ at at^{-1}	^{129}I/^{236}U at at^{-1}
Station 1	TU1141-H160122	5	ENACW	35.16	16.49	250	7.2 ± 0.1	9.2 ± 0.4	1130 ± 60	7.9 ± 0.4
40°19.99′ N	TU1151-H160120	25	ENACW	35.50	15.09	262	7.4 ± 0.1	10.6 ± 0.8	1330 ± 100	7.0 ± 0.5
10°2.16′ W	TU1152-H160119	50	ENACW	35.70	13.76	254	8.2 ± 0.1	9.2 ± 0.5	1110 ± 60	8.9 ± 0.5
Bottom depth: 3536 m	TU1153-H160118	100	ENACW	35.74	13.03	239	8.3 ± 0.1	8.4 ± 0.4	1100 ± 50	9.9 ± 0.5
	TU1154-H160110	200	ENACW	35.71	12.50	228	7.5 ± 0.1	8.9 ± 0.5	1050 ± 60	8.5 ± 0.5
	TU1147-H160103	400	ENACW	35.65	11.63	212	6.6 ± 0.1	8.6 ± 0.5	1030 ± 70	7.7 ± 0.5
	TU1134-H160080	1000	MW	36.15	11.13	177	3.4 ± 0.1	8.3 ± 0.4	1000 ± 60	4.1 ± 0.2
	TU1135-H160079	1200	MW	36.11	10.42	182	3.1 ± 0.1	8.4 ± 0.4	990 ± 60	3.7 ± 0.2
	TU1136-H160078	1600	MW/LSW	35.52	6.74	220	3.1 ± 0.1	10.0 ± 0.6	1010 ± 60	3.1 ± 0.2
	TU1123-H160077	2000	LSW	35.09	4.07	248	2.1 ± 0.1	7.9 ± 0.4	940 ± 50	2.6 ± 0.1
	TU1124-H160076	2500	NEADW$_L$	35.00	3.16	246	1.0 ± 0.1	2.5 ± 0.6	340 ± 110	4.1 ± 0.9
	TU1125-H160075	3000	NEADW$_L$	34.95	2.60	244	0.2 ± 0.2	2.3 ± 0.3	270 ± 30	0.9 ± 0.9
	TU1126-H160074	3506	NEADW$_L$	34.92	2.28	243	0.2 ± 0.2	4.4 ± 0.3	540 ± 40	0.5 ± 0.5
Surface 1	TU1148-H160123	5	ENACW				7.0 ± 0.1	9.3 ± 0.4	1160 ± 50	7.5 ± 0.4
40°19.98′ N										
9°27.57′ W										
Station 13	TU1155-H160211	10	ENACW	35.85	15.55	259	8.5 ± 0.3	8.5 ± 0.4	950 ± 40	10.0 ± 0.5
41°2298′ N	TU1156-H160085	30	ENACW	35.83	15.00	259	7.7 ± 0.3	8.6 ± 0.3	980 ± 40	8.9 ± 0.5
13°53.26′ W	TU1158-H160061	65	ENACW	35.76	13.16	251	7.9 ± 0.3	8.8 ± 0.4	1010 ± 50	8.9 ± 0.5
Bottom depth: 5347 m	TU1159-H160084	120	ENACW	35.74	12.84	247	7.6 ± 0.3	8.8 ± 0.3	1030 ± 40	8.6 ± 0.5
	TU1160-H160083	250	ENACW	35.69	12.39	245	8.0 ± 0.3	8.8 ± 0.3	1030 ± 40	9.1 ± 0.5
	TU1149-H160082	800	IcSPMW	35.72	10.51	182	4.9 ± 0.3	8.3 ± 0.3	980 ± 40	5.9 ± 0.4
	TU1137-H160081	1150	IcSPMW	35.86	9.45	188	3.9 ± 0.2	8.7 ± 0.3	970 ± 40	4.4 ± 0.3
	TU1127-H160073	2000	LSW	35.03	3.82	258	2.6 ± 0.2	6.3 ± 0.3	720 ± 40	4.2 ± 0.4
	TU1129-H160072	3000	NEADW$_L$	34.95	2.65	249	0.2 ± 0.2	1.2 ± 0.2	140 ± 20	2 ± 2
	TU1130-H160071	4000	NEADW$_L$	34.91	2.19	243	0.2 ± 0.2	0.3 ± 0.2	40 ± 20	6 ± 7
	TU1131-H160070	4885	NEADW$_L$	34.90	2.05	243	0.5 ± 0.1			
	TU1132-H160069	5334	NEADW$_L$	34.90	2.04	244	1.6 ± 0.1			
Surface 2	TU1161-H160215	5	ENACW				8.9 ± 0.3	8.5 ± 0.4	990 ± 40	10.4 ± 0.6
44°43.46′ N										
18°10.34′ W										
Station 21	TU1162-H160124	5	ENACW	35.69	14.45	277	8.7 ± 0.2	8.6 ± 0.5	990 ± 60	10.2 ± 0.6
46°32.65′ N	TU1163-H160214	12	ENACW	35.69	14.45	277	9.1 ± 0.3	8.5 ± 0.4	970 ± 50	10.7 ± 0.6
19°40.32′ W	TU1164-H160213	50	ENACW	35.62	12.72	266	9.9 ± 0.3	8.5 ± 0.4	980 ± 50	11.6 ± 0.6
Bottom depth: 4515 m	TU1165-H160121	100	ENACW	35.66	12.52	254	8.8 ± 0.2	8.1 ± 0.3	940 ± 40	10.9 ± 0.5
	TU1166-H160212	200	ENACW	35.64	12.03	248	9.8 ± 0.3	8.4 ± 0.4	960 ± 40	11.7 ± 0.6
	TU1170-H160104	450	ENACW	35.51	11.06	252	10.3 ± 0.2	9.1 ± 0.5	1060 ± 60	11.2 ± 0.6
	TU1167-H160105	800	IcSPMW	35.31	9.03	188	8.6 ± 0.2	8.6 ± 0.4	980 ± 40	10.0 ± 0.5
	TU1168-H160096	1500	LSW	35.00	4.40	259	8.4 ± 0.2	7.9 ± 0.5	970 ± 60	10.6 ± 0.6
	TU1138-H160068	2300	LSW	34.92	3.22	273	5.5 ± 0.2	7.9 ± 0.3	930 ± 40	7.0 ± 0.4
	TU1150-H160067	2750	ISOW	34.94	2.86	267	4.4 ± 0.2	6.4 ± 0.3	780 ± 40	6.8 ± 0.5
	TU1133-H160066	4000	NEADW$_L$	34.92	2.22	242	0.6 ± 0.2	0.6 ± 0.2	80 ± 20	9 ± 4
	TU1139-H160065	4474	NEADW$_L$	34.91	2.16	240	1.1 ± 0.2	0.6 ± 0.2	80 ± 20	17 ± 6
Surface 3	TU1171-H160219	5	ENACW				10.9 ± 0.4	7.9 ± 0.4	920 ± 50	13.9 ± 0.8
47°17.39′ N										
20°15.71′ W										
Station 26	TU1172-H160125	5	ENACW	35.31	11.52	282	13.3 ± 0.2	8.8 ± 0.4	1000 ± 50	15.1 ± 0.7
50°16.67′ N	TU1173-H160218	25	ENACW	35.31	11.52	282	12.9 ± 0.3	8.2 ± 0.5	950 ± 60	16 ± 1
22°36.28′ W	TU1174-H160217	50	ENACW	35.19	9.85	291	16.7 ± 0.3	8.1 ± 0.5	970 ± 60	21 ± 1
Bottom depth: 4130 m	TU1205-H160117	100	ENACW	35.17	9.45	284	19.2 ± 0.3	8.1 ± 0.3	940 ± 40	23.7 ± 0.9
	TU1206-H160216	250	SAIW	35.14	8.67	265	20.4 ± 0.4	9.3 ± 0.4	1060 ± 40	21.9 ± 0.9
	TU1188-H160111	500	IcSPMW	34.99	6.69	211	15.9 ± 0.3	8.3 ± 0.4	970 ± 50	19 ± 1
	TU1183-H160106	1000	LSW	34.96	4.40	263	13.4 ± 0.2	8.2 ± 0.4	1020 ± 50	16.3 ± 0.9
Surface 4	TU1184-H160222	5	SAIW				14.9 ± 0.3	7.8 ± 0.4	890 ± 50	19 ± 1
52°7.99′ N										
24°3.50′ W										
Station 32	TU0971-H160126	5	SAIW	35.07	10.16	292	19.9 ± 0.3	7.4 ± 0.6	870 ± 80	27 ± 2
55°30.336′ N	TU1200-H160221	30	SAIW	35.06	10.02	292	20.5 ± 0.4	8.1 ± 0.3	950 ± 40	25 ± 1
26°42.62′ W	TU1207-H160116	60	SAIW	35.14	8.85	288	18.9 ± 0.3	9.2 ± 0.3	1040 ± 40	20.6 ± 0.7
Bottom depth: 3235 m	TU1208-H160220	150	SAIW	35.11	8.11	274	20.1 ± 0.4	8.3 ± 0.3	980 ± 40	24.1 ± 0.9
	TU1175-H160097	380	SAIW	35.04	6.70	222	15.7 ± 0.3	8.0 ± 0.4	970 ± 50	19.5 ± 0.9
	TU1201-H160098	600	IcSPMW	34.96	5.02	246	17.8 ± 0.3	9.0 ± 0.2	1060 ± 30	19.8 ± 0.6
	TU1176-H160099	850	LSW	34.93	4.32	267	15.8 ± 0.3	9.1 ± 0.4	1097 ± 50	17.3 ± 0.8
	TU1202-H160112	1200	LSW	34.91	3.84	277	18.5 ± 0.3	9.7 ± 0.3	1130 ± 40	19.1 ± 0.6
	TU1177-H160113	1700	LSW	34.93	3.55	272	12.3 ± 0.2	8.8 ± 0.4	1030 ± 50	14.1 ± 0.7
	TU1178-H160064	2250	LSW	34.93	3.11	274	10.7 ± 0.3	8.1 ± 0.3	960 ± 40	13.2 ± 0.6
	TU1179-H160063	2650	ISOW	34.96	2.84	271	10.5 ± 0.2	8.0 ± 0.4	920 ± 50	13.2 ± 0.7
	TU1180-H160062	3220	ISOW	34.96	2.53	263	13.2 ± 0.3	7.0 ± 0.3	820 ± 40	18.8 ± 0.9

Table 1. Continued.

Station and location	ETH code	Depth m	Dominant water mass	Salinity	Potential temp. °C	Oxygen µmol kg^{-1}	^{129}I $\times 10^7$ at kg^{-1}	^{236}U $\times 10^6$ at kg^{-1}	$^{236}U/^{238}U$ $\times 10^{-12}$ at at^{-1}	$^{129}I/^{236}U$ at at^{-1}
Station 38	TU1189-H160230	5	IcSPMW	35.06	9.24	296	16.7 ± 0.3	8.7 ± 0.4	1030 ± 50	19 ± 1
58°50.56′ N	TU1190-H160229	20	IcSPMW	35.06	9.23	296	16.7 ± 0.3	9.8 ± 0.3	1170 ± 50	17.0 ± 0.7
31°15.97′ W	TU1193-H160228	60	IcSPMW	35.08	7.95	291	17.4 ± 0.3	8.8 ± 0.3	1010 ± 40	19.7 ± 0.8
Bottom depth: 1345 m	TU1203-H160227	110	IcSPMW	35.10	7.45	273	18.7 ± 0.4	8.7 ± 0.3	1010 ± 40	21.4 ± 0.9
	TU1204-H160226	300	IcSPMW	35.11	7.19	273	19.1 ± 0.4	9.0 ± 0.2	1040 ± 30	21.3 ± 0.7
	TU1209-H160225	650	IcSPMW	35.06	5.94	234	15.5 ± 0.3	9.3 ± 0.3	1050 ± 40	16.6 ± 0.7
	TU1210-H160224	1000	LSW	34.99	4.33	262	18.3 ± 0.4	9.6 ± 0.2	1070 ± 30	19.1 ± 0.6
	TU1213-H160223	1336	ISOW	34.99	3.90	267	21.4 ± 0.5	9.3 ± 0.3	1100 ± 40	23 ± 1
Surface 5	TU1194-H160277	5	IrSPMW				16.8 ± 0.3	8.9 ± 0.4	1030 ± 40	19.0 ± 0.8
59°16.77′ N										
35°33.64′ W										
Station 44	TU1217-H160276	5	IrSPMW	34.85	6.86	318	19.4 ± 0.3	9.4 ± 0.3	1120 ± 40	20.6 ± 0.8
59°37.36′ N	TU1260-	5	IrSPMW	34.85	6.86	318		9 ± 3	1040* ± 330	
38°57.234′ W	TU1195-H160275	20	IrSPMW	34.85	6.85	318	17.2 ± 0.3	9.9 ± 0.4	1170 ± 50	17.4 ± 0.8
Bottom depth: 2929 m	TU1218-H160274	40	IrSPMW	34.88	4.62	306	20.9 ± 0.3	9.2 ± 0.3	1090 ± 40	22.8 ± 0.9
	TU1219-H160273	80	IrSPMW	34.90	4.30	295	19.5 ± 0.3	9.1 ± 0.3	1070 ± 40	21.5 ± 0.7
	TU1196-H160272	150	IrSPMW	34.90	4.05	298	18.4 ± 0.3	9.2 ± 0.3	1090 ± 40	20.0 ± 0.8
	TU1220-H160271	300	LSW	34.90	3.94	298	22.5 ± 0.4	9.9 ± 0.3	1130 ± 30	22.8 ± 0.7
	TU1221-H160253	850	LSW	34.87	3.62	292	24.5 ± 0.4	9.6 ± 0.7	1160 ± 80	25 ± 2
	TU1185-H160254	1400	LSW	34.93	3.57	273	10.5 ± 0.2	9.2 ± 0.4	1070 ± 50	11.4 ± 0.5
	TU1186-H160255	1800	LSW	34.93	3.26	274	14.3 ± 0.2	9.5 ± 0.3	1070 ± 40	15.1 ± 0.5
	TU1191-H160256	2250	ISOW	34.93	2.86	276	15.5 ± 0.3	8.6 ± 0.3	1000 ± 40	18.0 ± 0.7
	TU1248-H160308	2600	ISOW	34.92	2.44	282	38.7 ± 0.6	10 ± 1	1180* ± 130	40 ± 4
	TU1261-H160307	2875	DSOW	34.88	1.17	308	98 ± 2	9 ± 4	1090* ± 420	110 ± 40
	TU1262-H160306	2909	DSOW	34.89	1.06	309	99 ± 2	11 ± 3	1280* ± 310	90 ± 20
Station 53	TU1265-H160285	5	PIW	31.90	−0.68	423	256 ± 4	16 ± 2	2050* ± 310	160 ± 20
59°53.86′ N	-H160284	25	PIW	32.10	−1.18	417	247 ± 5			
43°0.33′ W	TU1267-H160283	50	PIW	32.95	−1.52	364	236 ± 8	12 ± 4	1570* ± 510	200 ± 60
Bottom depth: 193 m										
Station 60	TU1214-H160282	5	IrSPMW	34.83	6.94	325	19.0 ± 0.3	8.9 ± 0.2	1040 ± 30	21.4 ± 0.6
59°47.96′ N	TU1197-H160281	25	IrSPMW	34.98	6.56	314	17.0 ± 0.3	8.6 ± 0.3	1030 ± 40	19.6 ± 0.7
42°00.78′ W	TU1192-H160280	50	IrSPMW	35.01	6.27	303	16.6 ± 0.3	8.3 ± 0.5	1020 ± 60	20 ± 1
Bottom depth: 1719 m	TU1198-H160279	100	IrSPMW	35.02	5.97	291	17.1 ± 0.3	8.9 ± 0.3	1020 ± 40	19.3 ± 0.7
	TU1224-H160278	200	IrSPMW	34.96	5.20	287	18.4 ± 0.3	8.9 ± 0.4	1030 ± 50	20.8 ± 0.9
	TU1215-H160268	500	IrSPMW	34.94	4.45	280	22.8 ± 0.5	9.5 ± 0.4	1140 ± 50	24 ± 1
	TU1216-H160257	750	IrSPMW	34.90	3.85	286	21.3 ± 0.4	9.3 ± 0.3	1120 ± 40	22.8 ± 0.8
	TU1225-H160258	1000	LSW	34.92	3.77	278	23.1 ± 0.5	13 ± 2	1600* ± 210	18 ± 2
	TU1229-H160259	1190	LSW/ISOW	34.93	3.61	277	25.6 ± 0.4	9.5 ± 0.9	1210* ± 120	27 ± 3
	-H160260	1500	LSW/ISOW	34.92	3.16	281	30.3 ± 0.5			
	TU1242-H160305	1672	LSW/ISOW	34.92	3.00	281	36.1 ± 0.6	9 ± 1	1100* ± 180	40 ± 6
	TU1243-H160304	1712	LSW/ISOW	34.91	2.94	284	37.4 ± 0.6	8.7 ± 0.9	1080* ± 120	43 ± 5
Station 61	TU1263-H160296	5	SAIW	32.40	0.07	412	219 ± 4	15 ± 3	1940 ± 340	140 ± 30
59°45.21′ N	-H160290	25	SAIW	32.63	−0.41	402	244 ± 4			
45°6.74′ W	TU1269-H160289	50	SAIW	32.81	−0.65	383	251 ± 4			
Bottom depth: 144 m										
Station 64	TU1236-H160288	5	IrSPMW	34.81	6.71	317	24.7 ± 0.4	9 ± 1	1060* ± 160	29 ± 4
59°4.30′ N	TU1226-H160287	25	IrSPMW	34.81	6.68	317	21.5 ± 0.4	12 ± 1	1370* ± 140	19 ± 2
46°5.29′ W	TU1227-H160286	50	IrSPMW	34.86	6.13	319	18.4 ± 0.3	11 ± 1	1480* ± 180	16 ± 2
Bottom depth: 2473 m	TU1230-H160261	100	IrSPMW	34.95	5.37	294	22.2 ± 0.4	11 ± 1	1390* ± 140	20 ± 2
	-H160262	200	IrSPMW	34.94	4.79	289	29.2 ± 0.5			
	TU1231-H160267	450	LSW	34.92	4.22	288	26.8 ± 0.5	9 ± 1	1080* ± 140	30 ± 4
	TU1232-H160100	900	LSW	34.87	3.60	295	24.7 ± 0.4	7.9 ± 0.8	970* ± 100	31 ± 3
	-H160088	1150	LSW	34.91	3.71	281	23.7 ± 0.4			
	TU1222-H160089	1400	LSW	34.93	3.55	274	21.0 ± 0.3	9.8 ± 0.3	1130 ± 40	21.3 ± 0.7
	TU1238-H160090	1800	LSW	34.92	3.05	278	27.7 ± 0.4	9 ± 1	1070* ± 120	31 ± 4
	TU1228-H160303	2150	ISOW	34.93	2.70	278	20.9 ± 0.3	11 ± 1	1300* ± 150	19 ± 2
	TU1249-H160302	2462	DSOW	34.90	2.15	291	56.2 ± 0.9	9.5 ± 0.9	1160* ± 110	60 ± 6
Surface 6	TU1239-H160231	5	LSW				30.9 ± 0.5			
56°44.79′ N										
47°31.31′ W										
Station 69	-H160232	5	LSW	34.62	6.24	326	48.8 ± 0.8			
55°50.50′ N	TU1254-H160233	25	LSW	34.67	3.72	324	49.9 ± 0.8	9 ± 3	1060 ± 350	60 ± 20
48°5.59′ W	TU1264-H160234	50	LSW	34.79	3.78	297	41.8 ± 0.7	5 ± 3	640* ± 320	80 ± 40
Bottom depth: 3678 lm	-H160239	100	LSW	34.83	3.81	296	32.9 ± 0.6			
	TU1240-H160	200	LSW	34.84	3.62	298	29.8 ± 0.5	9 ± 2	1080* ± 190	32 ± 6
	TU1272101-H160	500	LSW	34.86	3.49	296	29.3 ± 0.5	7 ± 2	820* ± 290	40 ± 20
	TU1273-H109160	1000	LSW	34.85	3.39	296	26.0 ± 0.4			
	TU1274-H160092	1800	LSW	34.92	3.57	274	17.6 ± 0.3	5 ± 2	620* ± 300	30 ± 20
	TU1275-H160241	2200	LSW	34.92	3.22	275	20.0 ± 0.4	8 ± 3	940* ± 330	26 ± 9
	TU1233-H160093	2800	ISOW	34.92	2.70	279	24.5 ± 0.4	8.9 ± 0.9	1070* ± 110	28 ± 3
	TU1251-H160301	3500	ISOW	34.91	1.75	294	72 ± 1	15 ± 2	1770* ± 270	49 ± 8
	TU1255-H160300	3659	DSOW	34.90	1.47	299	85 ± 1	19 ± 3	2230* ± 340	44 ± 7

Table 1. Continued.

Station and location	ETH code	Depth m	Dominant water mass	Salinity	Potential temp. °C	Oxygen µmol kg^{-1}	^{129}I $\times 10^7$ at kg^{-1}	^{236}U $\times 10^6$ at kg^{-1}	^{236}U/^{238}U $\times 10^{-12}$ at at^{-1}	^{129}I/^{236}U at at^{-1}
Surface 53°40.18′ N 49°29.49′ W	7 TU1277-H160269	5	LSW				31.6 ± 0.5	10.2 ± 0.5	1220 ± 70	31 ± 2
Surface 8 52°46.17′ N 51°48.26′ W	TU1278-H160270	5	SAIW/PIW				71 ± 1	15.7 ± 0.9	2090 ± 140	45 ± 3
Station 77 52°59.98′ N 51°6.01′ W Bottom depth: 2522 m	TU1245-H160242	5	LSW	34.47	7.28	324	37.9 ± 0.6	9 ± 1	1040* ± 170	45 ± 7
	-H160243	25	LSW	34.63	5.30	334	32.2 ± 0.6			
	TU1279-H160244	50	LSW	34.74	3.57	312	32.3 ± 0.6	10.4 ± 0.4	1230 ± 50	31 ± 1
	TU1246-H160245	100	LSW	34.79	3.42	304	32.4 ± 0.6	9 ± 1	1040* ± 170	38 ± 6
	TU1280-H160246	200	LSW	34.83	3.46	299	30.9 ± 0.5	10.4 ± 0.4	1210 ± 50	30 ± 1
	TU1281-H160102	650	LSW	34.86	3.46	294	27.0 ± 0.4	10.3 ± 0.4	1190 ± 50	26 ± 1
	TU1284-H160247	950	LSW	34.87	3.41	294	24.1 ± 0.4	10.6 ± 0.3	1240 ± 50	22.7 ± 0.8
	TU1234-H160094	1250	LSW	34.91	3.54	279	22.8 ± 0.4	9.5 ± 0.9	1130* ± 100	24 ± 2
	TU1282-H160299	1700	LSW	34.92	3.12	276	21.7 ± 0.4	9.8 ± 0.5	1140 ± 70	22 ± 1
	TU1285-H160095	2200	ISOW	34.92	2.60	280	35.5 ± 0.6	10.6 ± 0.3	1270 ± 50	34 ± 1
	TU1252-H160298	2477	ISOW	34.91	2.18	285	48.7 ± 0.8	8 ± 3	1030* ± 310	60 ± 20
	TU1286-H160297	2500	ISOW	34.91	2.09	287	47.0 ± 0.8	12.1 ± 0.6	1400 ± 70	39 ± 2
Station 78 51°59.33′ N 53°40.01′ W Bottom depth: 377 m	TU1256-H160248	5	PIW	31.79	5.17	342	75 ± 1	16 ± 4	2110* ± 500	50 ± 10
	TU1257-H160249	25	PIW	32.86	−0.57	452	77 ± 1	19 ± 3	2350* ± 370	41 ± 6
	TU1270-H160250	50	PIW	33.06	−1.46	340	74 ± 1	12 ± 4		60 ± 20
	TU1258-H160251	200	PIW	34.08	0.77	308	64 ± 1	11 ± 2	1380* ± 280	60 ± 10
	TU1287-H160252	367	PIW	34.62	2.92	283	44.2 ± 0.8	11.2 ± 0.5	1350 ± 70	40 ± 2

3 Results and discussion

3.1 Water mass structure in 2014

The water mass structure in spring 2014 is described using the zonal sections for salinity, potential temperature and dissolved oxygen concentrations (Fig. 2) to facilitate the understanding of ^{129}I and ^{236}U distributions in Sect. 3.2. The assessment of the water mass structure from GEOVIDE was performed using an extended optimum multi-parameter analysis (OMP) (further details are found in García-Ibáñez et al., 2018).

In the upper water column (< 500 m), warm and saline Central Water dominates the eastern part of the section between the coast off Portugal and station 26 (Fig. 2a and b). Central Water (or eastern North Atlantic Central Water, ENACW) is characterised by the highest potential temperatures and relatively high salinities, as they have been transported from subtropical latitudes into the eastern part of the section by the north-east-flowing branches of the NAC. Part of the ENACW recirculates into the Iceland Basin and the Irminger Sea, where air–sea fluxes transform them into colder and fresher SPMWs (McCartney and Talley, 1982) that occupy equivalent depths between the subarctic front (SAF; roughly at 22.5° W, station 26) and Greenland (Fig. 2a and b). The upper water column on the continental shelves and slopes of Greenland and Canada is occupied by PIW, which presents very low salinities (< 34) and potential temperatures usually < 0 °C (Fig. 2a and b). PIW originates from the Arctic Ocean, enters through the Fram (PIW–Atlantic) and Nares Straits (PIW–Canada), and joins the shallow western boundary transport in the EGC and LC (Fig. 1).

At intermediate depths, LSW is the most abundant water mass and fills the entire section from the upper waterlevels to about 2000 m depth (Fig. 2). LSW is formed in the Labrador Sea and, to a lesser extent, in the Irminger Sea by transformation of SPMWs via winter convection (e.g. Jong and Steur, 2016). Then, it flows south as part of the DBWC (e.g. Bersch et al., 2007) or east into the Irminger, Iceland and West European basins (Fig. 1). LSW is characterised by a relative minimum in salinity (< 34.9) and temperature (∼ 3 °C) at its formation region, and warmer and saltier values as it mixes with surrounding waters along its equatorward and eastward transport (Fig. 2a and b). Station 26 is also affected by the Subarctic Intermediate Water (SAIW), which presents lower salinities (∼ 34.9) and potential temperatures (4–7 °C) than the other water masses surrounding it at similar depths, i.e. ENACW and SPMW from the Iceland Basin (IcSPMW; Fig. 2a and b). SAIW forms in the western boundary of the SPNA (i.e. the LC) by mixing between LSW and subtropical waters carried by the NAC (Arhan, 1990; Read, 2000), before subducting at about 400 m depth and being advected within the northern branch of the NAC (Fig. 2). Depths around 1000 m in the WEB (stations 1 and 13) are also influenced by the northward-flowing Mediterranean Water (MW) (Fig. 1), which is characterised by a maximum in salinity (> 36) and minimum in oxygen (∼ 180 µmol kg^{-1}) (Fig. 2a and c).

In the deep-water column (> 2000 m), the lower northeastern Atlantic Deep Water (NEADW$_L$) dominates the section in the WEB (east of 20° W), while in the western part, the most abundant water masses are the dense overflow waters. NEADW$_L$ is generally saltier, colder and older than the overlying LSW due to the major contribution of the northward-flowing Antarctic Bottom Water (AABW)

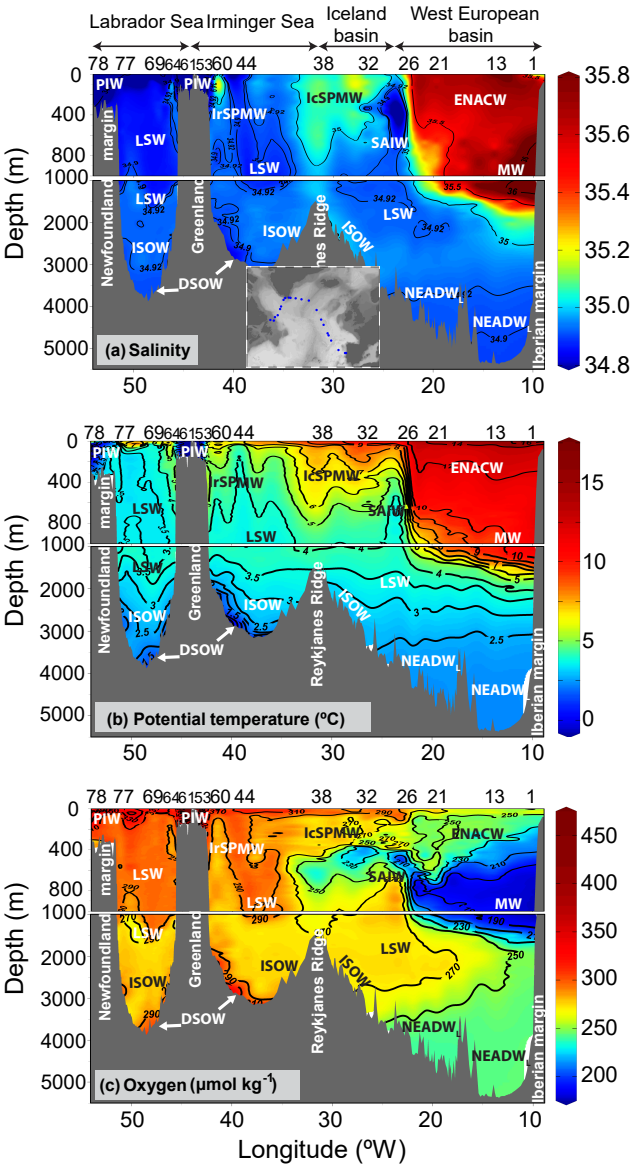

Figure 2. Vertical distribution of **(a)** salinity, **(b)** potential temperature and **(c)** dissolved oxygen along the GEOVIDE section in spring 2014. Water mass acronyms are defined in the Appendix.

(Fig. 2a–c). Dense overflow waters dominate the bottom depths on both sides of the Reykjanes Ridge and in the Irminger and Labrador seas (Fig. 1). ISOW is best identified thanks to its local salinity maximum (∼ 34.92) on the flanks of the Reykjanes Ridge and between the LSW and DSOW in the Irminger and Labrador seas (Fig. 2a). This water mass is produced by mixing old Norwegian Sea waters that overflow the Iceland–Scotland sill and entrain SPMW and LSW in the SPNA (e.g. van Aken and De Boer, 1995). ISOW mainly flows along the eastern flank of the Reykjanes Ridge into the Irminger and Labrador seas (Fig. 1), yet an increasing number of studies point towards the eastward return flow of this water mass through passages in the Mid-Atlantic Ridge (Xu et al., 2018) or directly along the flanks of the Rockall Plateau into the eastern part of the GEOVIDE section (e.g. Zou et al., 2017) (Fig. 1). Finally, DSOW is present between ISOW and the seafloor in the Irminger and Labrador seas (notably stations 44 and 69). This overflow water can be distinguished from ISOW by its lower salinities (< 34.90), potential temperatures (< 2 °C) and higher oxygen concentration (> 290 µmol kg^{-1}) (Fig. 2a–c) due to the more recent ventilation and rapid advective flow of DSOW from the formation region north of the Denmark Strait into the GEOVIDE section (e.g. Read, 2000) (Fig. 1).

3.2 The relationship of ^{129}I and ^{236}U with water masses in 2014

The concentrations of ^{129}I and ^{236}U, and atom ratios of ^{236}U/^{238}U and ^{129}I/^{236}U are reported in Table 1. Detailed depth profiles for these radionuclides are displayed along with salinity, potential temperature and dissolved oxygen concentrations in the Supplement (Fig. S1). The ^{129}I concentrations range from $(0.20 \pm 0.20) \times 10^7$ to $(256 \pm 4) \times 10^7$ at kg^{-1}. The ^{236}U/^{238}U ratios range from $(40 \pm 20) \times 10^{-12}$ to $(2350 \pm 370) \times 10^{-12}$. The ^{129}I/^{236}U ratios range from 0.50 ± 0.50 to 200 ± 60.

The results from this study are best described in relation to the water mass structure described in Sect. 3.1, which has been represented with overlaid isohalines on the radionuclide distribution plots (Fig. 3). The ^{129}I concentrations (Fig. 3a) and ^{236}U/^{238}U ratios (Fig. 3b) are generally higher west of ∼ 25°W in southward flowing waters than in northward-flowing low-latitude waters dominating the eastern SPNA. This is also clear when comparing tracer values of stations 1–26 with those from stations 32–78 (Table 1). Such general radionuclide distribution is largely due to the fact that southward-flowing northern waters are located downstream of Sellafield and La Hague, and therefore present additional radionuclide contributions (especially for ^{129}I) from these facilities. The highest ^{129}I concentrations (∼ 250×10^7 at kg^{-1}) and ^{236}U/^{238}U ratios (∼ 2300×10^{-12}) are present in PIW and RAW carried by the EGC and LC over the shelves and slopes of Greenland and Canada. This water admixture, largely influenced by NRPs (e.g. Alfimov et al., 2013), can mix with DSOW precursor waters through winter convection in the Greenland Sea (e.g. Gascard et al., 2002) or directly intrude DSOW by cascading in the Labrador Sea (e.g. Falina et al., 2012). Consequently, the DSOW core, found at the lowermost 100 m in the Irminger and Labrador seas, presents ^{129}I concentrations in the (85–100) $\times 10^7$ at kg^{-1} range and ^{236}U/^{238}U ratios of (1300–2300) $\times 10^{-12}$, which is in agreement with high radionuclide levels previously reported for DSOW (Casacuberta et al., 2014; Orre et al., 2010; Smith et al., 2005, 2016). Intermediate ^{129}I concentrations ((5–50) $\times 10^7$ at kg^{-1}) and ^{236}U/^{238}U ratios ((500–1500) $\times 10^{-12}$) characterize the wa-

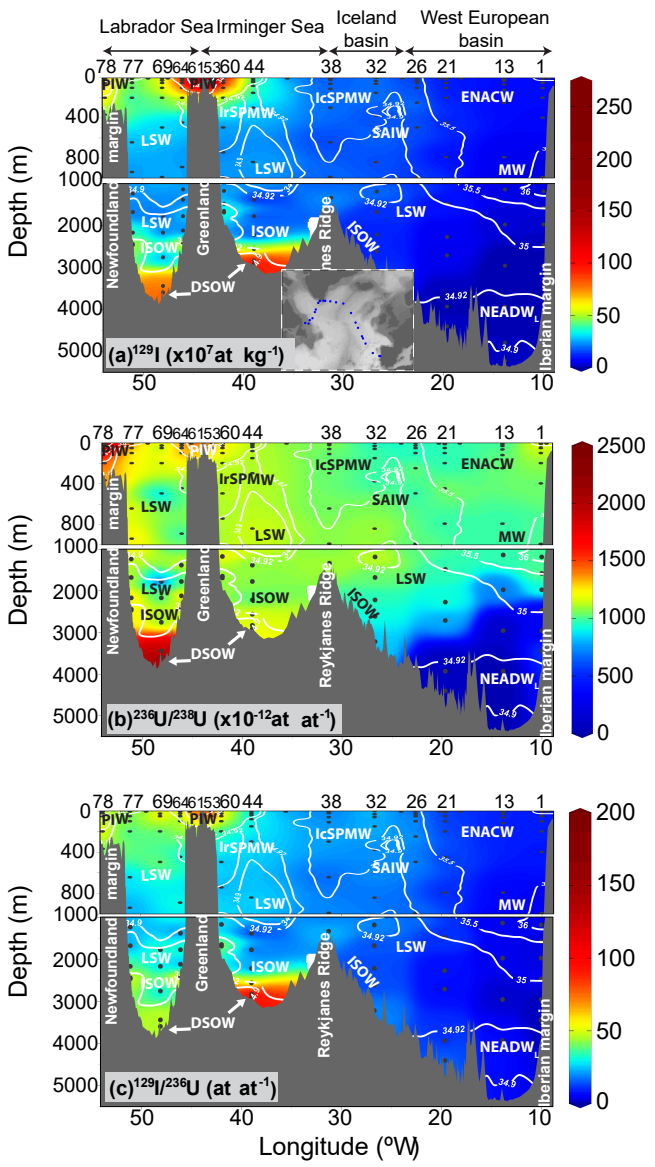

Figure 3. Vertical distribution of **(a)** ^{129}I concentrations, and atom ratios of **(b)** ^{236}U/^{238}U and **(c)** ^{129}I/^{236}U during the GEOVIDE cruise in spring 2014. Isohalines are overlaid to represent the water mass distribution. Acronyms are defined in the Appendix.

ter masses that fill most of the remaining GEOVIDE section. In the upper 500 m, ENACWs record rather uniform ^{129}I concentrations ($\sim 10 \times 10^7$ at kg^{-1}) and ^{236}U/^{238}U ratios ($\sim 1000 \times 10^{-12}$) in the WEB (stations 1 to 21). The ^{129}I concentrations of SPMWs located further west almost double those of ENACW (^{236}U/^{238}U ratios are similar), indicating that ENACW may be influenced by effluents from NRPs while recirculating in the northern SPNA or in the Nordic seas. SAIW also presents relatively high ^{129}I concentrations ($\sim 20 \times 10^7$ at kg^{-1}) at stations 26 and 32, probably because of the influence of waters carried by the LC. The 500–2000 m layer is dominated by LSW, which displays a wide range of ^{129}I concentrations ((5–50) $\times 10^7$ at kg^{-1}) and ^{236}U/^{238}U ratios ((700–1250) $\times 10^{-12}$), with values decreasing downstream from its formation regions, the Labrador and Irminger seas. Similar depths are also influenced by MW (stations 1 and 13), yet its ^{129}I concentrations ($\sim 3 \times 10^7$ at kg^{-1}) and ^{236}U/^{238}U ratios ($\sim 1000 \times 10^{-12}$) were significantly lower in 2014 than average ^{129}I concentrations (9×10^7 at kg^{-1}) and ^{236}U/^{238}U ratios (1600×10^{-12}) reported in the outflow region of MW at the Strait of Gibraltar in 2013 (Castrillejo et al., 2017). Thus, 2014 data probably reflect the dilution of MW, which is largely affected by input from the Marcoule nuclear facility (Castrillejo et al., 2017), with old LSW and SPMW carrying a diluted NRP signal. The deeper parts of the section west of 20° W and below 2000 m are influenced by ISOW, which is characterised by relatively high ^{129}I concentrations ((10–70) $\times 10^7$ at kg^{-1}) and ^{236}U/^{238}U ratios ((900–1700) $\times 10^{-12}$). The lowest ^{129}I concentrations ((0.2–2.0) $\times 10^7$ at kg^{-1}) and ^{236}U/^{238}U ratios ((40–350) $\times 10^{-12}$) are found at depths greater than 2000 m in the WEB and are associated with NEADW$_L$ (stations 1 to 13).

The distribution of ^{129}I/^{236}U (Fig. 3c) is notably driven by ^{129}I concentrations, which display a greater range (3 orders of magnitude) than the ^{236}U/^{238}U ratios (2 orders of magnitude). As noted before, this is probably due to the influence of NRPs, which released about 60 times more mass of ^{129}I than of ^{236}U to the North Atlantic (further discussion in Sect. 3.3). Thus, following the ^{129}I patterns described above, the ^{129}I/^{236}U ratios are particularly high (> 20) in the western part of the section and particularly contrasted in the Irminger and Labrador seas as discussed in Sect. 3.3 (Fig. 3c). The highest ^{129}I/^{236}U ratios (> 100) are present in waters transported by the shallow EGC and LC. Overflow waters are also distinguished by their relatively high ^{129}I/^{236}U ratios (60 to 110 for DSOW, 15 to 40 for ISOW).

3.3 Sources of ^{129}I and ^{236}U in the SPNA

All samples show ^{129}I concentrations and ^{236}U/^{238}U ratios well above the lithogenic background (LB) or the natural values ($\sim 0.04 \times 10^7$ at kg^{-1} for ^{129}I, Snyder et al., 2010; and 10^{-14}–10^{-13} for ^{236}U/^{238}U atom ratios: Christl et al., 2012 and Steier et al., 2008). This was also shown in previous studies, highlighting the influence of artificial sources on the presence of ^{129}I (e.g. Edmonds et al., 2001) and ^{236}U (Casacuberta et al., 2014; Christl et al., 2012) in the North Atlantic.

As in earlier studies (Casacuberta et al., 2016), we can estimate the contribution to our samples from the LB, GF and NRP by combining the ^{129}I/^{236}U and ^{236}U/^{238}U in a dual tracer approach (Fig. 4). This is possible because the atom ratios of ^{129}I/^{236}U and ^{236}U/^{238}U display a wide range of values due to the different inputs of ^{129}I and ^{236}U from the three sources. For example, the GF introduced about 10 times more ^{236}U than ^{129}I; thus this endmember is characterised by ^{129}I/^{236}U < 1 and ^{236}U/^{238}U surface ratios in the (1000–

2000) $\times 10^{-12}$ range. On the contrary, the total amount of ^{236}U introduced from European NRPs was much smaller than for ^{129}I. Therefore, a water mass with the additional influence of the European NRPs may present ^{129}I/^{236}U in the 1–350 range and ^{236}U/^{238}U above the GF. The natural presence of ^{129}I and ^{236}U is negligible compared to artificial sources, yet the LB can be distinguished by a very small ^{236}U/^{238}U ($\sim 10^{-13}$) and a relatively large ^{129}I/^{236}U ($\sim$ 370). The simple mixing model (Fig. 4) considers the three aforementioned endmembers constant in time, for which values were estimated by Casacuberta et al. (2016) based on the literature or on their own calculations. The mixing lines between each endmember represent all possible binary mixing scenarios; i.e. they delimit the range of ^{129}I/^{236}U and ^{236}U/^{238}U that a given water mass may show depending on the sources and on the different degrees of mixing. For instance, a sample falling in the 1 % value on the GF-NRP binary mixing line would be composed of waters largely carrying GF and about 1 % of the NRPs signal.

On top of the mixing model, we represent the results from the GEOVIDE cruise (Fig. 4). Each data point represents a seawater sample collected at a certain station (Fig. 4a) or assigned to a dominant water mass (Fig. 4b to f). The results show that most of the samples fall along the GF-NRP binary mixing line with contributions from NRPs > 1 %. The largest NRP contribution, above 5 %, is observed in the Irminger and Labrador seas, notably associated with PIW, DSOW and to lesser extent with ISOW. LSW also records NRP contributions > 1 % in the westernmost stations (e.g. 44 to 77), while LSW that has been transported further east on the section (stations 1 to 38) reflects the greater mixing or dilution with waters notably carrying GF. ENACWs are closer to the GF endmember, yet they show significant contributions (> 1 %) from NRP. This result is unexpected given that the transport of ENACW occurs upstream and far away from the NRPs, from subtropical latitudes into the eastern SPNA (stations 1 to 26). At least six samples are separated from the GF-NRP mixing line and plotted towards the LB endmember. These are associated with the contribution of the northward flowing AABW to NEADW$_L$ (van Aken and Becker, 1996). AABW is the oldest water mass in the SPNA and has little or no influence from nuclear activities given that it was not exposed to the surface or atmosphere for decades.

3.4 Time evolution of ^{129}I in the SPNA

In this section we compare radionuclide concentrations reported in the literature with those measured at nearby stations during GEOVIDE (Fig. 5). The assessment of the temporal evolution of radionuclide distributions is important to identify the main circulation features highlighted by these tracers. The limited data on the novel ^{236}U tracer prevent from studying any temporal evolution. In the case of ^{129}I, the existing time series for the central Labrador Sea (1993–2013, Fig. 5a) demonstrated that most of the tracer transport was carried by overflow waters (e.g. DSOW) and that the temporal evolution of ^{129}I concentrations in those waters could be associated with the tracer release from the European NRPs a few years earlier (Edmonds et al., 2001; Orre et al., 2010; Smith et al., 2005, 2016). For instance, the literature on ^{129}I shows a rise in tracer concentrations due to the increased ^{129}I discharge rate from European NRPs in the whole water column, being more pronounced (increase of about 10 times) in overflow waters (Fig. 5a). The depth distribution of ^{129}I concentrations in the Labrador Sea in 2014 (station 69) displays ^{129}I concentrations in DSOW about 15 % lower (see Sect. 3.5.4) than in 2012–2013 (Smith et al., 2016), yet the general shape of the depth profile is comparable (Fig. 5a). The main difference between the ^{129}I depth profiles in the Irminger Sea (station 44, red squares in Fig. 5a) and central Labrador Sea (station 69, red circles in Fig. 5a) in 2014 is the surface ^{129}I peak in the latter one. Considering the 30 m deep freshwater surface layer observed between station 69 and Greenland (not shown here), we suggest that waters carried by the West Greenland Current (continuation of the EGC) may have separated from the main western boundary transport and entered the central Labrador Sea (Cuny and Rhines, 2002). This may also explain the peak in ^{236}U/^{238}U ratios observed at the same location (Fig. S1).

A similar assessment of ^{129}I concentrations is now possible for the water column over the Reykjanes Ridge (station 38) and the Icelandic Basin (station 32) (Fig. 5b), which were first studied in 1993 (Edmonds et al., 2001). The ^{129}I concentrations in the water column are 5–7 times higher in 2014 than in 1993. The most pronounced increase occurs in the upper 1000 m filled by SPMWs and in the deep Icelandic Basin dominated by ISOW. This novel result shows that the ^{129}I tracer could potentially be used to trace the transformation of ENACWs into SPMWs and the evolution of ISOW. The depth profiles of ^{129}I concentration measured in the WEB in 2014 (particularly station 21) resemble the one sampled at the Porcupine Abyssal Plain (PAP) in 2012 by Vivo-Vilches et al. (2018) (Fig. 5c). The ^{129}I distribution in the upper 1000 m at PAP is very similar to station 21, located 365 km to the south-west, while below that depth ^{129}I concentrations are about 2.5×10^7 at kg^{-1} higher in the PAP. These results suggest a similar water mass composition for that region, yet the offset in deep ^{129}I concentrations would support the hypothesis that effluents from the nearby Sellafield and/or La Hague NRPs may directly enter the SPNA without previous circulation in the Nordic seas (see Sect. 3.5.1).

3.5 Tracing water mass circulation in the SPNA using ^{129}I and ^{236}U

We use the above information on the distribution, sources and time evolution of ^{129}I and ^{236}U to investigate the circulation of nuclear reprocessing effluents and in return, provide more insight into composition, spreading pathways and transport timescales of water masses in the SPNA.

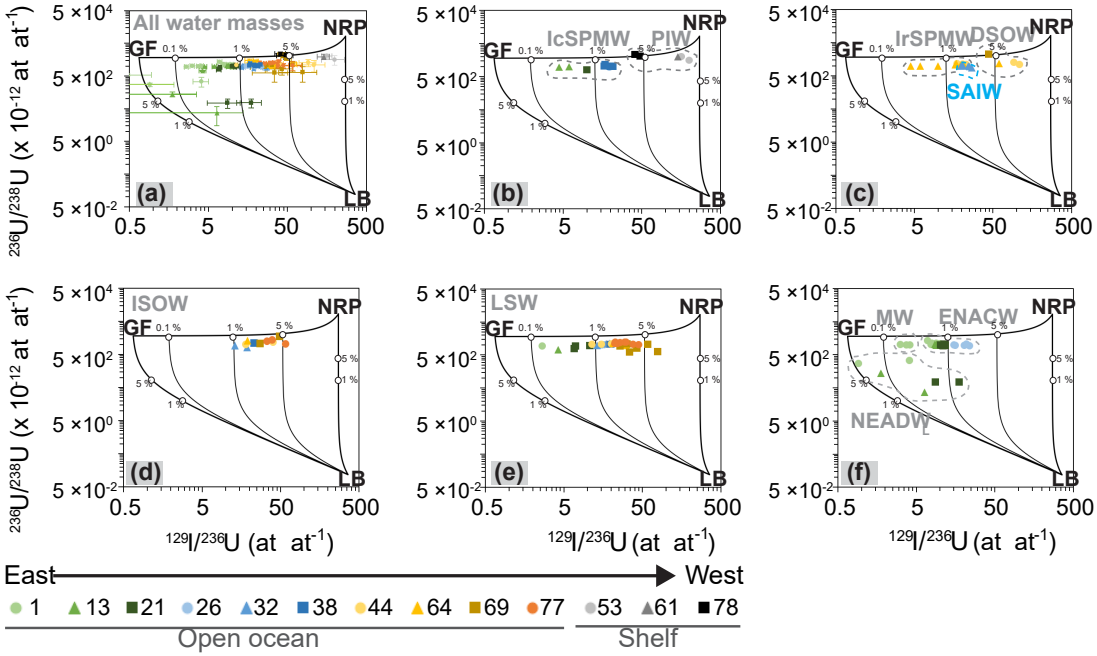

Figure 4. ^{129}I/^{236}U and ^{236}U/^{238}U atom ratios obtained during the GEOVIDE cruise in spring 2014 plotted on top of a binary mixing model (details in Sect. 3.3) to estimate the contribution from the three sources to the subpolar North Atlantic (global fallout, GF; European nuclear fuel reprocessing plants, NRP; and the natural or lithogenic background, LB). Data are plotted for **(a)** each station, and **(b–f)** for the main water masses described in Sect. 3.1. Diagram **(a)** also shows the data uncertainties. An explanation on how to interpret the results is provided in Sect. 3.3. Further detail about the binary mixing model can be found in the original study (Casacuberta et al., 2016). Water mass acronyms are defined in the Appendix.

3.5.1 Shallow water circulation in the eastern SPNA

The main transport of reprocessing effluents occurs poleward, yet the increasing observations and simulations on ^{129}I suggest that part of the NRP signal may directly enter the surface of the SPNA without previous circulation in the Nordic seas. This hypothesis is based on the fact that ^{129}I concentrations in surface waters of the north-eastern SPNA can record values more than 1 order of magnitude above the GF level (2.5×10^7 at kg^{-1}; Edmonds et al., 1998). He et al. (2013b) proposed that the outflow through the English Channel and the Irish Sea may lead to ^{129}I concentrations in surface waters above 20×10^7 at kg^{-1} and modify the isotopic iodine composition in the Bay of Biscay. Modelling of ^{129}I releases from the European NRPs also shows that tracers discharged from Sellafield may expand southwards (Villa et al., 2015), which could explain ^{129}I concentrations of 77×10^7 at kg^{-1} measured in surface waters of the Celtic Sea (Vivo-Vilches et al., 2018). GEOVIDE data (Table 1) of ^{129}I concentrations ($\sim 10 \times 10^7$ at kg^{-1}) and ^{129}I/^{236}U ratios (7–20) in ENACWs confirm the influence from the NRPs. If that was the case, the different NAC branches could mix ENACWs with reprocessing-labelled local waters and be transported southward by surface currents (e.g. Lambelet et al., 2015; Lherminier et al., 2010; Ríos et al., 1992). Indeed, NAC branches west of station 21 recirculated anti-cyclonically into the WEB, bringing waters south across the GEOVIDE section in 2014 (Zunino et al., 2017). Further, the transformation of ENACW into SPMW results in ^{129}I concentrations twice larger in the Icelandic Basin than in the WEB (Fig. 5b and c), which suggests the near-surface transport of ^{129}I from European NRPs also occurs southward across Iceland and Scotland. Consequently, ^{129}I concentrations in shallow waters at stations 1, 13 and 21 strongly contrast with those at stations 26 and 32 located west of the SAF (Table 1). Such near surface tracer input would also explain the increase in surface ^{129}I concentrations (Fig. S2) up to 10^8–10^9 at kg^{-1} in the Icelandic Basin and north-west of the British Isles by 2010–2012 (Gómez-Guzmán et al., 2013; Vivo-Vilches et al., 2018). Thus, one could potentially use ^{129}I to trace ENACWs in the upper water column of the WEB and their transformation into SPMW. This is not clearly supported by ^{236}U levels ($\sim 10 \times 10^6$ at kg^{-1}), which are close to GF in the shallow eastern SPNA, yet European NRPs introduced about 60 times less ^{236}U than ^{129}I (Christl et al., 2015b).

3.5.2 Shallow water transport and cascading in the Irminger Sea and Labrador Sea

It is well known that the eastern coast of Greenland receives RAW and PIW–Atlantic injected in the EGC (Fig. 1). Similarly, the shelf of Newfoundland is bathed by the LC,

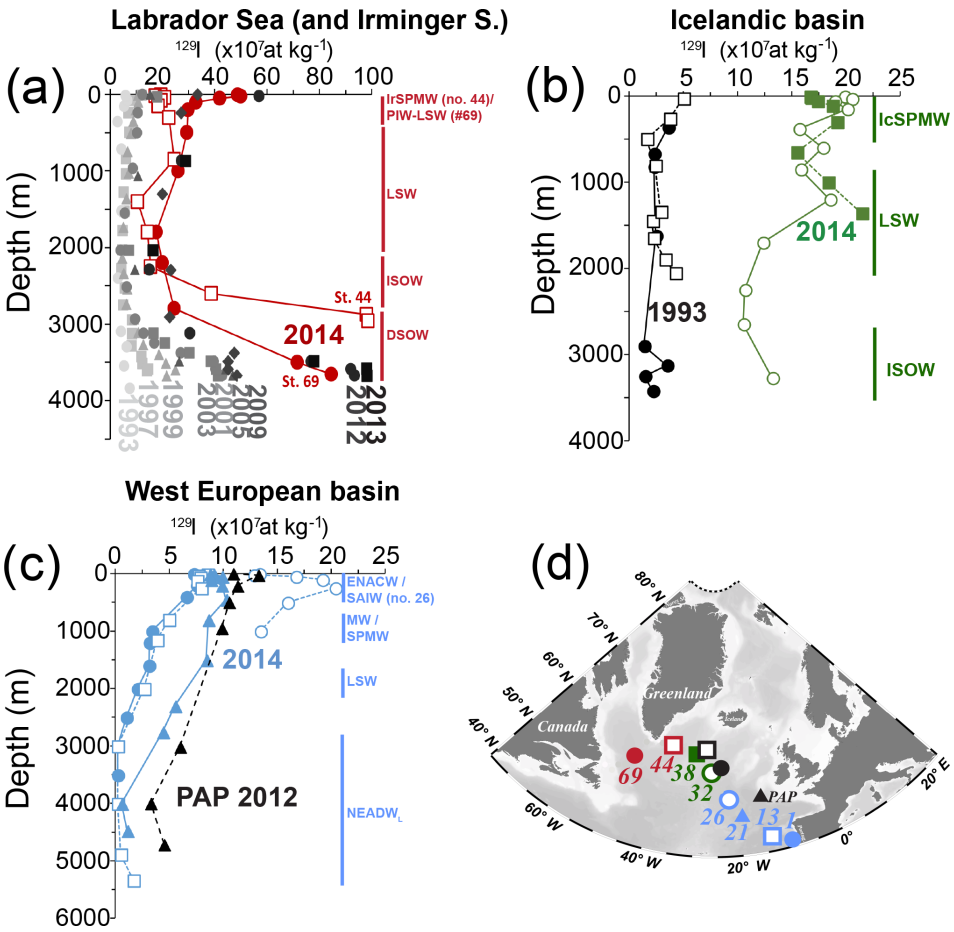

Figure 5. Vertical profiles of ^{129}I concentrations at locations shown in **(d)** of selected GEOVIDE stations and of those reported in nearby locations by earlier studies. **(a)** ^{129}L in the Labrador and Irminger seas, red profiles represent data from this work (2014). Data from 1993 were reported south-west of the GEOVIDE station 69 by Edmonds et al. (2001). Data from 1997 to 2013 were reported at station 17 of the AR7W line: for 1997, 1999 and 2001 by Smith et al. (2005); for 2003, 2005 and 2009 by Orre et al. (2010); and for 2012 and 2013 by Smith et al. (2016). **(b)** In the Icelandic Basin, green profiles show data from GEOVIDE stations 32 and 38 in 2014, while black profiles represent data from 1993 reported by Edmonds et al. (2001). **(c)** In the West European Basin, blue profiles represent data from GEOVIDE stations 1 to 26, while data from 2012 in the Porcupine Abyssal Plain (PAP) were reported by Vivo-Vilches et al. (2018). Water masses found during GEOVIDE cruise have been summarised and represented in same colour as the ^{129}I concentration profiles. Acronyms are defined in the Appendix.

which carries EGC waters and PIW–Canada, this last one being supplied through the Nares Strait (Curry et al., 2014). The tracer levels are particularly high in waters residing on the shelves, slopes and very deep waters around Greenland and Newfoundland (Fig. 3). Further, the tracer content differs between Arctic waters of Atlantic and Canadian origin, enriched in ^{129}I and ^{236}U, respectively. Thus, one may use them to distinguish key circulation features such as the EGC–LC and the DWBC in the Labrador and Irminger seas (Fig. 1). For example, at shallow depths, the EGC (stations 53 to 64) presents remarkably high ^{129}I concentrations (up to $\sim 250 \times 10^7$ at kg^{-1}) and ^{129}I/^{236}U ratios (up to 200), while both values are significantly lower in the LC (station 78), which is characterised by comparably higher ^{236}U/^{238}U ratios (up to 2350×10^{-12}) (Fig. 3). Differences on the composition of ^{129}I and ^{236}U in the two shallow boundary currents are likely due to the fact that waters of Atlantic origin (PIW–Atlantic and RAW) have been largely influenced by NRP effluents (high ^{129}I). On the contrary, the LC records lower ^{129}I concentrations due to the influence of PIW–Canada waters with a mainly GF signal (Ellis and Smith, 1999; Smith et al., 1998), and a large ^{236}U content (^{236}U/^{238}U ratios are likely $> 2000 \times 10^{-12}$) from both the GF and unconstrained Arctic river inputs (Casacuberta et al., 2016).

Shelf waters carried by the EGC are thought to occasionally descend down the Greenland slope feeding the East Greenland Spill Jet and DSOW (von Appen et al., 2014; Falina et al., 2012; Harden et al., 2014; Koszalka and Haine, 2013; Pickart et al., 2005; Rudels et al., 1999a). The GEOVIDE section shows a rise of ^{129}I concentrations at cer-

tain depths on the Greenland slope (e.g. station 60; Figs. 3 and S1), and particularly in bottom waters of the Irminger Sea (station 44), which are probably related to the cascading of ^{129}I-rich waters from the Greenland Shelf. This finding would be supported by OMP analyses that estimate up to 20 % of PIW in the DSOW realm (García-Ibáñez et al., 2018). Our results also highlight that similar processes may be taking place in the Canadian shelf, but with PIW–Canada water cascading to the bottom of the Labrador Sea. This would explain the slightly higher ^{236}U/^{238}U ratios near the Newfoundland Shelf (station 77; Figs. 3 and S1) compared to the offshore waters in the Labrador Sea (e.g. station 69) as well as the higher ^{236}U/^{238}U ratios and lower ^{129}I concentrations in the deep Labrador Sea (influenced by PIW–Canada) compared to the Irminger Sea (influenced by PIW–Atlantic) (Figs. 3 and 5a).

3.5.3 Spreading pathways of ISOW in the eastern SPNA

The ^{129}I and ^{236}U tracers may help to validate current interpretations of ISOW-spreading pathways in the SPNA which are largely based on model outputs or on limited observations (Fleischmann et al., 2001; LeBel Jr. et al., 2008; Xu et al., 2010; Zou et al., 2017). The ISOW is best distinguished by its relative ^{129}I concentration maxima and ^{129}I/^{236}U ratios of 15–40 due to NRPs, which are significantly higher than in surrounding waters (e.g. LSW, NEADW$_L$). This is particularly visible for ^{129}I concentrations (Fig. 5b and c, and Table 1) in deeper parts of the Icelandic Basin (stations 32 and 38) and the WEB (stations 1 and 13), where the presence of ISOW has also been inferred from OMP analyses (García-Ibáñez et al., 2018). For ^{236}U (Fig. S1), this increase is not as pronounced as for ^{129}I, probably due to the pre-existing ^{236}U from the GF. In the coming years, one can expect a stronger ^{129}I signal carried by ISOW because tracer concentrations in ISOW precursor waters have increased from 7×10^7 to 63×10^7 at kg^{-1} at the Iceland–Scotland sill from 1993 to 2012 in response to releases from the NRPs (Alfimov et al., 2013; Edmonds et al., 2001; Vivo-Vilches et al., 2018). The overflow of ISOW through the Iceland–Scotland sill has increasing implications for the deep ventilation of the SPNA and for the magnitude of the AMOC (García-Ibáñez et al., 2018). Thus, future time series of time-varying ^{129}I concentrations at GEOVIDE stations and further upstream may also be used to investigate timescales of ISOW ventilation in the North Atlantic Ocean.

3.5.4 Transit times and dilution factors of reprocessing-labelled Atlantic waters

The observations of ^{129}I concentrations in DSOW filling the central Labrador Sea between 1993 and 2013 (Fig. 5a) have also been valuable to estimate transport times of Atlantic waters carrying the NRP signal into the Arctic and the North Atlantic (Orre et al., 2010; Smith et al., 2005, 2011, 2016). The ^{129}I time series shows two tracer pulses, one in the late 1990s and the following about 10 years later (Fig. 6a, data points). Smith et al. (2005) suggested that the first sharp increase in ^{129}I concentrations in DSOW was related to the arrival of the tracer front observed in the mid-1990s at 60° N in the northern North Sea. The second peak in ^{129}I concentrations has also been related to the same cause as in the late 1990s front, but in this case, it would correspond to the return flow of AWs that were transported northwards into the Arctic Ocean before returning to the western SPNA (Smith et al., 2011). According to these authors, the 10-year gap between the two tracer fronts would be related to this Arctic loop, i.e. the transport of AWs by the FSBW into the Arctic Eurasian Basin, the return flow along the Lomonosov Ridge and the incorporation via the EGC into DSOW.

To test this hypothesis, we took the ^{129}I input function at 60° N for the northern North Sea (Fig. 6a, green dashed line) used in previous studies (e.g. Christl et al., 2015b; Orre et al., 2010; Smith et al., 2005). This input function is estimated assuming that the signal of both NRP mixtures in the North Sea and then is advected to 60° N in 2 years from La Hague and in 4 years from Sellafield. Following earlier modelling studies (Smith et al., 2005), we first estimate a new ^{129}I input function for DSOW in the central Labrador Sea (Fig. 6a, blue line) that should match the aforementioned first tracer front shown by ^{129}I measurements between 1993 and 2001 (Edmonds et al., 2001; Smith et al., 2005). This is achieved by applying a time lag (6 years) that accounts for the transit time from 60° N, and a dilution factor (DF = 50) that represents the mixing with waters carrying only the GF signal. Secondly, we estimate a second ^{129}I input function (Fig. 6a, red line) that fits the ^{129}I concentrations measured in 2012 and 2013 by Smith et al. (2016) and in 2014 by this study. We found that this is possible when the tracer input function (Fig. 6a, green dashed line) is diluted 30 times and a delay time of about 14 years is applied. Thus, 2014 data reported in this study support the current interpretation on the Arctic loop (e.g. Smith et al., 2016) and suggests that the second ^{129}I front probably peaked before the GEOVIDE cruise. Note that the latter input function (Fig. 6a, red line) only provides an upper estimate for the ^{129}I transit times and the dilution factor because the observed ^{129}I concentrations in 2012–2014 also contain water from the shorter loop (Fig. 6a, blue line). According to our results (Fig. 6a), AWs follow at least two paths before arriving at the Labrador Sea: (i) one short path into the Nordic Sea and then to the SPNA, which takes approximately 8–10 years from the NRPs, and (ii) a long path

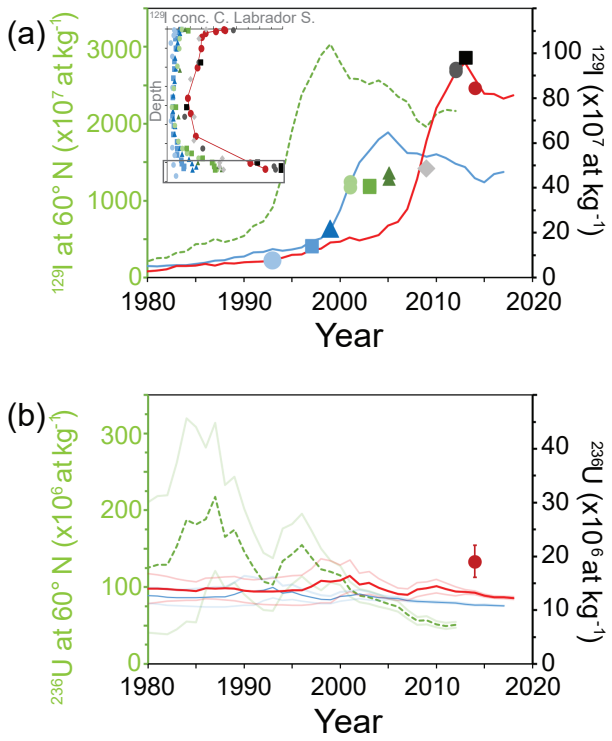

Figure 6. Comparison between measured (data points) and simulated (lines) radionuclide concentrations in bottom waters (DSOW) at the central Labrador Sea for **(a)** ^{129}I and **(b)** ^{236}U. The green *y* axis on the left represents radionuclide concentrations over time (or the radionuclide input functions, also in green) at 60° N due to releases from the European nuclear reprocessing plants and which were reported by Christl et al. (2015b). Note that for ^{236}U, the average input function is accompanied with a lower and upper bound estimate to acknowledge the current uncertainties on the ^{236}U releases from Sellafield and La Hague (Christl et al., 2015b). The black *y* axis on the right represents radionuclide concentrations, measured or simulated, in bottom waters of the central Labrador Sea. On these axes are the blue and red lines that represent two versions of the radionuclide input function at 60° N after dilution (DF = 50 and 30) and application of a time delay (6 and 14 years) that corresponds to the transport from 60° N to the central Labrador Sea. The blue and red simulations include background concentrations for ^{129}I (2.5×10^7 at kg^{-1}; Edmonds et al., 2001) and ^{236}U (10×10^6 at kg^{-1}; e.g. Christl et al., 2012) due to the global fallout. On the black *y* axis are also the radionuclide concentrations measured in 2014 that correspond to the bottom sample collected in GEOVIDE station 69. Earlier data on ^{129}I concentrations at similar locations were reported for 1993 by Edmonds et al. (2001); for 1997, 1999 and 2001 by Smith et al. (2005); for 2003, 2005 and 2009 by Orre et al. (2010); and for 2012 and 2013 by Smith et al. (2016).

which adds approximately 8 years of circulation in the Arctic Ocean, resulting in 16–18 years of transit time from the NRPs to the central Labrador Sea. A similar exercise for ^{236}U (Fig. 6b) shows that the single ^{236}U measurement available for overflow waters in the central Labrador Sea (2014, this work) is above the concentrations predicted using the two fits. Although the ^{236}U data would agree with the hypothesis of a second delayed ^{129}I pulse arriving from the Arctic Ocean, there are significant inconsistencies between the simulated and measured concentrations. These might be attributed to, among other factors, the large uncertainty of the used ^{236}U data point for 2014, uncertainties on the amount released by the Sellafield NRP (Christl et al., 2015), missing information on other sources or unaccounted-for features on the water mass circulation downstream of the NRPs.

4 Conclusions

The distribution of artificial ^{129}I and ^{236}U in the SPNA was governed by the main water mass circulation. The highest ^{129}I concentrations and ^{236}U/^{238}U ratios are associated with water masses originating from the Nordic seas (DSOW, ISOW and surface currents) or the Arctic Ocean (PIW). On the other end, ENACW and NEADW$_L$ transported from low latitudes north into the SPNA present ^{129}I concentrations and ^{236}U/^{238}U ratios of about 2–3 orders of magnitude lower. The ^{236}U/^{238}U–^{129}I/^{236}U dual tracer approach indicates that all water masses except NEADW$_L$ are influenced by GF and NRPs. ENACW is also influenced by effluents from NRPs (e.g. ^{129}I/^{236}U > 1), which suggests that part of the radioactive releases split off from the mainstream and enter the surface of the eastern SPNA either through direct exchange at the English Channel/Irish Sea or at the passage between Iceland and Scotland. Other key circulation features, such as the shallow transport of PIW and RAW by the EGC and LC or the deep North Atlantic ventilation by overflow waters (DSOW, ISOW), are particularly visible due to the presence of reprocessing ^{129}I and ^{236}U. For example, ISOW is tagged with relatively high ^{129}I and, therefore, it can be traced while spreading eastwards into the WEB among waters that have lower tracer amounts. The combined use of ^{236}U/^{238}U–^{129}I/^{236}U allows water mass composition and origin to be differentiated and serves to confirm known circulation features and validate recent interpretations on water mass transport pathways and timescales. For example, the LC mainly presents the GF signal and unconstrained Arctic river inputs (more ^{236}U relative to ^{129}I), indicating the contribution from PIW–Canada through the Canadian Archipelago, while the EGC, largely influenced by the NRPs (more ^{129}I relative to ^{236}U), indicates the contribution of RAW and PIW–Atlantic. The contribution of RAW/PIW–Atlantic and PIW–Canada to DSOW in the Irminger and Labrador seas is also visible thanks to slight elevations of tracer values in near bottom depths and specific ^{236}U/^{238}U–^{129}I/^{236}U ratios due to cascading events. This work also contributes to extend the existing ^{129}I time series in the Labrador Sea/Irminger Sea and allows a first assessment of time-varying ^{129}I concentrations east of Reykjanes Ridge. Increasing ^{129}I concentrations are observed in the western part of the GEOVIDE

section and in the Icelandic Basin. In the WEB, the short observation time (2012–2014) does not yet allow temporal trends of ^{129}I levels to be seen. The ^{129}I data in overflow waters of the central Labrador Sea (1993–2014) can be fitted with reprocessing ^{129}I (and ^{236}U) input functions following earlier modelling studies to better understand the transport timescales and dilution factors of AWs tagged by the NRP signal. This study supports the current interpretations on the circulation of AWs, which apparently follow a short loop trough the Nordic seas (8–10 years in this study) and a longer loop including the circulation in the Arctic Eurasian Basin (16–18 years in this study). Further experimental and modelling studies on ^{129}I and ^{236}U may confirm circulation features highlighted by these tracers and shed more light on novel findings such as the transport of ISOW in to the eastern SPNA, which plays an important role on the ventilation of the deep SPNA.

Data availability. Data are provided in Table 1. The ancillary data are found in the Supplement as an excel table.

Appendix A: Acronyms used to define water masses, geographic locations and radionuclide sources

AABW	Antarctic Bottom Water
AMOC	Atlantic meridional overturning circulation
AMS	Accelerator mass spectrometry
AW	Atlantic Water
BSBW	Barents Sea Branch Water
DSOW	Denmark Strait Overflow Water
DWBC	Deep Western Boundary Current
EGC	East Greenland Current
ENACW	Eastern North Atlantic Central Water
FSBW	Fram Strait Branch Water
GF	Global fallout
ISOW	Iceland–Scotland Overflow Water
LB	Lithogenic background
LC	Labrador Current
LH	La Hague
LSW	Labrador Sea Water
MW	Mediterranean Water
NAC	North Atlantic Current
NCC	Norwegian Coastal Current
$NEADW_L$	North East Atlantic Deep Water lower
NRP	Nuclear reprocessing plant
NwAC	Norwegian Atlantic Current
OMP	Optimum multi-parameter analysis
PAP	Porcupine Abyssal Plain
PIW	Polar Intermediate Water
RAW	Return Atlantic Water
SAF	Subarctic Front
SAIW	Subarctic Intermediate Water
SF	Sellafield
SPMW	Subpolar Mode Water
SPNA	Subpolar North Atlantic
WEB	West European Basin
WSC	West Spitsbergen Current

Supplement. The supplement related to this article is available online at: https://doi.org/10.5194/bg-15-5545-2018-supplement.

Author contributions. MC participated in the collection and analyses of samples and led the preparation of the manuscript. The work was supervised by PhD advisors PM, JGO and NC. The AMS determination of radionuclides was carried out by MC and CV. In addition, all co-authors contributed to the interpretation of the results and helped to elaborate the manuscript.

Competing interests. The authors declare that they have no conflict of interest.

Special issue statement. This article is part of the special issue "GEOVIDE, an international GEOTRACES study along the OVIDE section in the North Atlantic and in the Labrador Sea (GA01)". It is not associated with a conference.

Acknowledgements. We are grateful to the captain and crew of R/V *Pourquoi Pas?* as well as the technical team for their work at sea (Pierre Branellec, Floriane Desprez de Gésincourt, Michel Hamon, Catherine Kermabon, Philippe Le Bot, Stéphane Leizour, Olivider Ménage, Fabien Pérault, and Emmanuel de Saint-Léger). A big thank you is extended to Yi Tang for help with sampling and to Anita Schlatter for assistance in the laboratory. This manuscript has been notably improved thanks to the constructive comments from two anonymous reviewers. We give thanks to Jan Lukas Menzel and the group led by Eric Achterberg (GEOMAR, Kiel) for providing the FISH device to collect surface seawater. The work by Catherine Schmechtig with the LEFE CYBER database management is also acknowledged. Some of the ^{129}I data discussed from the literature were kindly provided by Vasily Alfimov, Henrietta Edmonds and John Norton Smith. Several figures were created using Ocean Data View (Schlitzer, 2017). We would also like to thank Natalie Dubois and Alfred Lück for providing the laboratory space and assistance at EAWAG. The GEOVIDE cruise was funded by the French National Research Agency (ANR-13-BS06-0014, ANR-12-PDOC-0025-01), the French National Center for Scientific Research (CNRS LEFE CYBER), the LabexMER (ANR-10-LABX-19), and Ifremer. This work was funded by the Ministerio de Economía y Competitividad of Spain (MDM2015-0552), the Generalitat de Catalunya (MERS 2017 SGR-1588) and consortium partners of the ETH Zurich Laboratory of Ion Beam Physics (EAWAG, EMPA, and PSI). Maxi Castrillejo was funded by a FPU PhD studentship (AP-2012-2901) from the Ministerio de Educación, Cultura y Deporte of Spain and the ETH Zurich Postdoctoral Fellowship Programme (17-2 FEL-30), co-funded by the Marie Curie Actions for People COFUND Programme. Núria Casacuberta's research was funded by the AMBIZIONE grant (PZ00P2_154805) from the Swiss National Science Foundation. Maribel I. García-Ibáñez was supported by the Spanish Ministry of Economy and Competitiveness through the BOCATS (CTM2013-41048-P) project co-funded by the Fondo Europeo de Desarrollo Regional 2014–2020 (FEDER).

Edited by: Catherine Jeandel
Reviewed by: two anonymous referees

References

Aarkrog, A., Dahlgaard, H., Hallstadius, L., Hansen, H., and Holm, E.: Radiocaesium from Sellafield effluents in Greenland waters, Nature, 304, 49–51, 1983.

Aarkrog, A., Boelskifte, S., Dahlgard, H., Duniec, S., Hallstadius, L., Holm, E., and Smith, J. N.: Technetium-99 and Cesium-134 as long distance tracers in Arctic Waters, Estuar. Coast. Shelf S., 24, 637–647, 1987.

Alfimov, V., Aldahan, A., Possnert, G., and Winsor, P.: Tracing water masses with ^{129}I in the western Nordic Seas in early Spring 2002, Geophys. Res. Lett., 31, L19305, https://doi.org/10.1029/2004GL020863, 2004.

Alfimov, V., Aldahan, A., and Possnert, G.: Water masses and ^{129}I distribution in the Nordic Seas, Nucl. Instrum. Meth. B, 294, 542–546, https://doi.org/10.1016/j.nimb.2012.07.042, 2013.

Arhan, M.: The North Atlantic Current and the subarctic intermediate water, J. Mar. Res., 48, 109–144, 1990.

Beasley, T., Cooper, L. W., Grebmeier, J. M., Aagaard, K., Kelley, J. M., and Kilius, L. R.: ^{237}Np/^{129}I Atom Ratios in the Arctic Ocean: Has ^{237}Np from Western European and Russian Fuel Reprocessing Facilities Entered the Arctic Ocean?, J. Environ. Radioactiv., 39, 255–277, 1998.

Bersch, M., Yashayaev, I., and Koltermann, K. P.: Recent changes of the thermohaline circulation in the subpolar North Atlantic, Ocean Dynam., 57, 223–235, https://doi.org/10.1007/s10236-007-0104-7, 2007.

Casacuberta, N., Christl, M., Lachner, J., van der Loeff, M. R., Masqué, P., and Synal, H.-A.: A first transect of ^{236}U in the North Atlantic Ocean, Geochim. Cosmochim. Ac., 133, 34–46, https://doi.org/10.1016/j.gca.2014.02.012, 2014.

Casacuberta, N., Masqué, P., Henderson, G., Rutgers van-der-Loeff, M., Bauch, D., Vockenhuber, C., Daraoui, A., Walther, C., Synal, H.-A., and Christl, M.: First ^{236}U data from the Arctic Ocean and use of ^{236}U/^{238}U and ^{129}I/^{236}U as a new dual tracer, Earth Planet. Sc. Lett., 440, 127–134, https://doi.org/10.1016/j.epsl.2016.02.020, 2016.

Casacuberta, N., Christl, M., Vockenhuber, C., Wefing, A.-M., Wacker, L., Masqué, P., Synal, H.-A., and Rutgers van der Loeff, M.: Tracing the three Atlantic branches entering the Arctic Ocean with ^{129}I and ^{236}U, J. Geophys, Res.-Oceans, https://doi.org/10.1029/2018JC014168, online first, 2018.

Castrillejo, M., Casacuberta, N., Christl, M., Garcia-Orellana, J., Vockenhuber, C., Synal, H.-A., and Masqué, P.: Anthropogenic ^{236}U and ^{129}I in the Mediterranean Sea: First comprehensive distribution and constrain of their sources, Sci. Total Environ., 593–594, 745–759, https://doi.org/10.1016/j.scitotenv.2017.03.201, 2017.

Christl, M., Lachner, J., Vockenhuber, C., Lechtenfeld, O., Stimac, I., van der Loeff, M. R., and Synal, H.-A.: A depth profile of uranium-236 in the Atlantic Ocean, Geochim. Cosmochim. Ac., 77, 98–107, https://doi.org/10.1016/j.gca.2011.11.009, 2012.

Christl, M., Lachner, J., Vockenhuber, C., Goroncy, I., Herrmann, J., and Synal, H. A.: First data of Uranium-236

in the North Sea, Nucl. Instrum. Meth. B, 294, 530–536, https://doi.org/10.1016/j.nimb.2012.07.043, 2013a.

Christl, M., Vockenhuber, C., Kubik, P. W., Wacker, L., Lachner, J., Alfimov, V., and Synal, H.: The ETH Zurich AMS facilities?: Performance parameters and reference materials, Nucl. Instrum. Meth. B, 294, 29–38, https://doi.org/10.1016/j.nimb.2012.03.004, 2013b.

Christl, M., Casacuberta, N., Lachner, J., Maxeiner, S., Vockenhuber, C., Synal, H. A., Goroncy, I., Herrmann, J., Daraoui, A., Walther, C., and Michel, R.: Status of ^{236}U analyses at ETH Zurich and the distribution of ^{236}U and ^{129}I in the North Sea in 2009, Nucl. Instrum. Meth. B, 361, 510–516, https://doi.org/10.1016/j.nimb.2015.01.005, 2015a.

Christl, M., Casacuberta, N., Vockenhuber, C., Elsässer, C., Bailly du Bois, P., Herrmann, J. jürgen and Synal, H.-A.: Reconstruction of the ^{236}U input function for the Northeast Atlantic Ocean: Implications for ^{129}I/^{236}U and ^{236}U/^{238}U-based tracer ages, J. Geophys. Res.-Oceans, 120, 11 https://doi.org/10.1002/2015JC011116, 2015b.

Christl, M., Casacuberta, N., Lachner, J., Herrmann, J., and Synal, H. A.: Anthropogenic ^{236}U in the North Sea – A Closer Look into a Source Region, Environ. Sci. Technol., 51, 12146–12153, https://doi.org/10.1021/acs.est.7b03168, 2017.

Cuny, J. and Rhines, P.-B.: Labrador Sea Boundary currents and the Fate of the Irminger Sea Water, Am. Met. Soc., 32, 627–647, 2002.

Curry, B., Lee, C. M., Petrie, B., Moritz, R. E., and Kwok, R.: Multiyear Volume, Liquid Freshwater, and Sea Ice Transports through Davis Strait, 2004-10, J. Phys. Oceanogr., 44, 1244–1266, 2014.

Dahlgaard, H.: Transfer of European Coastal Pollution to the Arctic?: Radioactive Tracers, Mar. Pollut. Bull., 31, 3–7, 1995.

Daniault, N., Mercier, H., Lherminier, P., Sarafanov, A., Falina, A., Zunino, P., Pérez, F. F., Ríos, A. F., Ferron, B., Huck, T., and Thierry, V.: The northern North Atlantic Ocean mean circulation in the early 21st century, Prog. Oceanogr., 146, 142–158, https://doi.org/10.1016/j.pocean.2016.06.007, 2016.

Doney, S. C. and Jenkins, W. J.: Ventilation of the deep western boundary current and abyssal western North Atlantic: Estimates from tritium and ^{3}He distributions, J. Phys. Oceanogr., 24, 638–659, 1994.

Edmonds, H. N., Smith, J. N., Livingston, H. D., Kilius, L. R., and Edmond, J. M.: ^{129}I in archived seawater samples, Deep-Sea Res. Pt. I, 45, 1111–1125, https://doi.org/10.1016/S0967-0637(98)00007-7, 1998.

Edmonds, H. N., Zhou, Z. Q., Raisbeck, G. M., Yiou, F., Kilius, L., and Edmond, J. M.: Distribution and behavior of anthropogenic ^{129}I in water masses ventilating the North Atlantic Ocean, J. Geophys. Res., 106, 6881–6894, 2001.

Ellis, K. M. and Smith, J. N.: The flow of radionuclides through the Canadian Archipelago, Proc. IAEA Mainre Pollut. Symp. IAEA Tech. Doc., 1094, 462–464, Monaco, 1999.

Falina, A., Sarafanov, A., Mercier, H., Lherminier, P., Sokov, A., and Daniault, N.: On the cascading of dense shelf waters in the Irminger Sea, J. Phys. Oceanogr., 42, 2254–2267, 2012.

Fleischmann, U., Hildebrandt, H., Putzka, A., and Bayer, R.: Transport of newly ventilated deep water from the Iceland Basin to the West European Basin, Deep-Sea Res., 48B, 1793–1819, 2001.

Fogelqvist, E. J., Blindheim, J., Tanhua, T. T., Osterhus, S., Buch, E., and Rey, F.: Greenland-Scotland overflow studied by hydrochemical multivariate analysis, Deep-Sea Res. Pt. I, 50, 73–102, 2003.

García-Ibáñez, M. I., Pérez, F. F., Lherminier, P., Zunino, P., Mercier, H., and Tréguer, P.: Water mass distributions and transports for the 2014 GEOVIDE cruise in the North Atlantic, Biogeosciences, 15, 2075–2090, https://doi.org/10.5194/bg-15-2075-2018, 2018.

Gascard, J., Watson, A. J., Messias, M.-J., Olsson, K. A., Johannessen, T., and Simonsen, K.: Long-lived vortices as a mode of deep ventilation in the Greenland Sea, Nature, 416, 525–527, 2002.

Gascard, J. C., Raisbeck, G., Sequeira, S., Yiou, F., and Mork, K. A.: The Norwegian Atlantic Current in the Lofoten Basin inferred from hydrological and tracer data (^{129}I) and its interaction with the Norwegian Coastal Current, Geophys. Res. Lett., 31, L01308, https://doi.org/10.1029/2003GL018303, 2004.

Gómez-guzmán, J. M., Villa, M., Le Moigne, F., López-gutiérrez, J. M., and García-león, M.: AMS measurements of ^{129}I in seawater around Iceland and the Irminger Sea, Nucl. Instrum. Meth. B, 294, 547–551, https://doi.org/10.1016/j.nimb.2012.07.045, 2013.

Hansen, B. and Osterhus, S.: North Atlantic – Nordic Sea exchanges, Prog. Oceanogr., 45, 109–208, 2000.

Harden, B. E., Pickart, R. S., and Benfrew, I. A.: Offshore Transport of Dense Water from the East Greenland Shelf, J. Phys. Oceanogr., 44, 229–245, https://doi.org/10.1175/JPO-D-12-0218.1, 2014.

He, P., Aldahan, a., Possnert, G., and Hou, X. L.: A summary of global ^{129}I in marine waters, Nucl. Instrum. Meth. B, 294, 537–541, https://doi.org/10.1016/j.nimb.2012.08.036, 2013a.

He, P., Hou, X., Aldahan, A., Possnert, G., and Yi, P.: Iodine isotopes species fingerprinting environmental conditions in surface water along the northeastern Atlantic Ocean, Sci. Rep.-UK, 3, 2685, https://doi.org/10.1038/srep02685, 2013b.

Holm, E., Persson, B. R. R., Hallstadius, L., Aarkrog, A., and Dahlgaard, H.: Radio-cesium and transuranium elements in the Greenland and Barents Seas, Oceanol. Acta, 6, 457–462, 1983.

Hou, X.: Application of ^{129}I as an Environmental Tracer, J. Radioanal. Nucl. Ch., 262, 67–75, 2004.

Jong, M. F. and Steur, L.: Strong winter cooling over the Irminger Sea in winter 2014–2015, exceptional deep convection, and the emergence of anomalously low SST, Geophy. Res. Lett., 43, 7106–7113, https://doi.org/10.1002/2016GL069596, 2016.

Karcher, M., Smith, J. N., Kauker, F., Gerdes, R., and Smethie, W. M.: Recent changes in Arctic Ocean circulation revealed by iodine-129 observations and modeling, J. Geophys. Res.-Oceans, 117, 1–17, https://doi.org/10.1029/2011JC007513, 2012.

Kershaw, P. and Baxter, A.: The transfer of reprocessing wastes from north-west Europe to the Arctic, Deep-Sea Res. Pt. II, 42, 1413–1448, 1995.

Koszalka, I. M. and Haine, T. W. N.: Fates and Travel Times of Denmark Strait Overflow Water in the Irminger Basin, J. Phys. Oceanogr., 43, 2611–2628, https://doi.org/10.1175/JPO-D-13-023.1, 2013.

Lambelet, M., van de Flierdt, T., Crocket, K., Rehkämper, M., Kreissig, K., Coles, B., Rijkenberg, M. J. A., Gerringa, L. J. A., de Baar, H. J. W., and Steinfeldt, R.: Neodymium isotopic composition and concentration in the western North Atlantic Ocean: results from the GEO-

TRACES GA02 section, Geochim. Cosmochim. Ac., 177, 1–29, https://doi.org/10.1016/j.gca.2015.12.019, 2016.

LeBel, D. A., Smethie Jr., W. M., Rhein, M., Kieke, D., Fine, R. A., Bullister, J. L., Min, D.-H., Roether, W., Weiss, R., Andrié, C., Smythe-Wright, D., and Jones, E. P. The formation rate of North Atlantic Deep Water and eighteen Degree water calculated from CFC-11 inventories observed during WOCE, Deep-Sea Res. Pt. I, 55, 891–910, https://doi.org/10.1016/j.dsr.2008.03.009, 2008.

Lherminier, P., Mercier, H., Huck, T., Gourcuff, C., Perez, F. F., Morin, P., Sarafanov, A., and Falina, A.: The Atlantic Meridional Overturning Circulation and the subpolar gyre observed at the A25-OVIDE section in June 2002 and 2004, Deep-Sea Res. Pt. I., 57, 1374–1391, https://doi.org/10.1016/j.dsr.2010.07.009, 2010.

McCartney, M. and Talley, L. D.: The Subpolar Mode Water of the North Atlantic Ocean, J. Phys. Oceanogr., 12, 1169–1188, 1982.

Mercier, H., Lherminier, P., Sarafanov, A., Gaillard, F., Daniault, N., Desbruyères, D., Falina, A., Ferron, B., Gourcuff, C., Huck, T., and Thierry, V.: Variability of the meridional overturning circulation at the Greenland–Portugal OVIDE section from 1993 to 2010, Prog. Oceanogr., 132, 250–261, https://doi.org/10.1016/j.pocean.2013.11.001, 2013.

Michel, R., Daraoui, A., Gorny, M., Jakob, D., Sachse, R., Tosch, L., Nies, H., Goroncy, I., Herrmann, J., Synal, H. A., Stocker, M., and Alfimov, V.: Iodine-129 and iodine-127 in European seawaters and in precipitation from Northern Germany, Sci. Total Environ., 419, 151–169, https://doi.org/10.1016/j.scitotenv.2012.01.009, 2012.

Orre, S., Smith, J. N., Alfimov, V., and Bentsen, M.: Simulating transport of ^{129}I and idealized tracers in the northern North Atlantic Ocean, Environ. Fluid Mech., 10, 213–233, 2010.

Pérez, F. F., Mercier, H., Vázquez-rodríguez, M., Lherminier, P., Velo, A., Pardo, P. C., Rosón, G., and Ríos, A. F.: Atlantic Ocean CO_2 uptake reduced by weakening of the meridional overturning circulation, Nat. Geosci., 6, 146–152, https://doi.org/10.1038/ngeo1680, 2013.

Pickart, R. S., Torres, D. J., and Fratantoni, P. S.: The East Greenland Spill Jet, J. Phys. Oceanogr., 58, 1037–1053, 2005.

Raisbeck, G. M. and Yiou, F.: ^{129}I in the oceans: origins and applications, Sci. Total Environ., 237–238, 31–41, 1999.

Raisbeck, G. M. and Yiou, F.: Use of ^{129}I as an oceanographic tracer in the Nordic Seas, Pap. Present. 5th Int. Conf. Environ. Radioact. Arct. Antarct., St. Petersburg, Russ., 127–130, 2002.

Raisbeck, G. M., Yiou, F., Zhou, Z. Q., and Kilius, L. R.: ^{129}I from nuclear fuel reprocessing facilities at Sellafield (U.K.) and La Hague (France); potential as an oceanographie tracer, J. Marine Syst., 6, 561–570, https://doi.org/10.1016/0924-7963(95)00024-J, 1995.

Read, J. F.: CONVEX-91: water masses and circulation of the Northeast Atlantic subpolar gyre, Prog. Oceanogr., 48, 461–510, https://doi.org/10.1016/S0079-6611(01)00011-8, 2000.

Ríos, A. F., Pérez, F. F., and Fraga, F.: Water masses in the upper and middle North Atlantic Ocean east of the Azores, Deep-Sea Res., 39, 645–658, 1992.

Rudels, B.: Arctic Ocean circulation, processes and water masses: A description of observations and ideas with focus on the period prior to the International Polar Year 2007–2009, Prog. Oceanogr., 132, 22–67, https://doi.org/10.1016/j.pocean.2013.11.006, 2015.

Rudels, B., Eriksson, P., Gronvall, H., Hietala, R., and Launiainen, J.: Hydrographic Observations in Denmark Strait in Fall 1997, and their Implications for the Entrainment into the Overflow Plume, Geophys. Res. Lett., 26, 1325–1328, 1999a.

Rudels, B., Friedrich, H. J., and Quadfasel, D.: The Arctic Circumpolar Boundary Current, Deep-Sea Res. Pt. II, 46, 1023–1062, https://doi.org/10.1016/S0967-0645(99)00015-6, 1999b.

Sakaguchi, A., Kawai, K., Steier, P., Quinto, F., Mino, K., Tomita, J., Hoshi, M., Whitehead, N., and Yamamoto, M.: First results on ^{236}U levels in global fallout, Sci. Total Environ., 407, 4238–4242, 2009.

Sakaguchi, A., Kadokura, A., Steier, P., Takahashi, Y., Shizuma, K., Hoshi, M., Nakakuki, T., and Yamamoto, M.: Uranium-236 as a new oceanic tracer: a first depth profile in the Japan Sea and comparison with caesium-137, Earth Planet. Sc. Lett., 333–334, 165–170, 2012.

Schlitzer, R.: Ocean Data View, available at: http://odv.awi.de (last access: September 2018), 2017.

Smith, J. N., Ellis, K. M., and Kilius, L. R.: ^{129}I and ^{137}Cs tracer measurements in the Arctic Ocean, Deep-Sea Res. Pt. I, 45, 959–984, https://doi.org/10.1016/S0967-0637(97)00107-6, 1998.

Smith, J. N., Jones, E. P., Moran, S. B., Smethie Jr., W. M., and Kieser, W. E.: Iodine-129/CFC-11 transit times for Denmark Strait Overflow Water in the Labrador and Irminger Seas, J. Geophys. Res., 110, 1–16, https://doi.org/10.1029/2004JC002516, 2005.

Smith, J. N., Mclaughlin, F. A., Smethie Jr., W. M., Moran, S. B., and Lepore, K.: Iodine-129, ^{137}Cs, and CFC-11 tracer transit time distributions in the Arctic Ocean, J. Geophys. Res., 116, 1–19, https://doi.org/10.1029/2010JC006471, 2011.

Smith, J. N., Smethie Jr., W. M., Yashayev, I., Curry, R., and Aztsu-Scott, K.: Time series measurements of transient tracers and tracer-derived transport in the Deep Western Boundary Current between the Labrador Sea and the subtropical Atlantic Ocean at line W, J. Geophys. Res.-Oceans, 121, 1–24, https://doi.org/10.1002/2016JC011759, 2016.

Snyder, G., Aldahan, A., and Possnert, G.: Global distribution and long-term fate of anthropogenic I-129 in marine and surface water reservoirs, Geochem. Geophys. Geosy., 11, Q04010, https://doi.org/10.1029/2009GC002910, 2010.

Steier, P., Bichler, M., Keith Fifield, L., Golser, R., Kutschera, W., Priller, A., Quinto, F., Richter, S., Srncik, M., Terrasi, P., Wacker, L., Wallner, A., Wallner, G., Wilcken, K. M. and Maria Wild, E.: Natural and anthropogenic ^{236}U in environmental samples, Nucl. Instrum. Meth. B, 266, 2246–2250, https://doi.org/10.1016/j.nimb.2008.03.002, 2008.

Sy, A., Rhein, M., Lazier, J., Koltermann, K., Meincke, J., Putzka, A., and Bersch, M.: Surprisingly rapid spreading of newly formed intermediate waters across the North Atlantic Ocean, Nature, 386, 675–679, 1997.

Tanhua, T., Bulsiewicz, K., and Rhein, M.: Spreading of overflow water from the Greenland to the Labrador Sea, Geophys. Res. Lett., 32, L10605, https://doi.org/10.1029/2005GL022700, 2005.

van Aken, H. M. and Becker, G.: Hydrography and through-flow in the northeastern North Atlantic Ocean: the NANSEN project, Prog. Oceanogr., 38, 297–346, 1996.

van Aken, H. M. and De Boer, C. J.: On the synoptic hydrography of intermediate and deep water masses in the Iceland Basin,

Deep-Sea Res. Pt. I, 42, 165–189, https://doi.org/10.1016/0967-0637(94)00042-Q, 1995.

Villa, M., López-Gutiérrez, J. M., Suh, K.-S., Min, B.-I., and Periañez, R.: The behaviour of ^{129}I released from nuclear fuel reprocessing factories in the North Atlantic Ocean and transport to the Arctic assessed from numerical modelling, Mar. Poll. Bull., 90, 15–24, https://doi.org/10.1016/j.marpolbul.2014.11.039, 2015.

Vivo-Vilches, C., López-Gutiérrez, J. M., Periáñez, R., Marcinko, C., Le Moigne, F., Mcginnity, P., Peruchena, J. I., and Villa-Alfageme, M.: Recent evolution of ^{129}I levels in the Nordic Seas and the North Atlantic Ocean, Sci. Total Environ., 621, 376–386, https://doi.org/10.1016/j.scitotenv.2017.11.268, 2018.

Vockenhuber, C., Casacuberta, N., Christl, M., and Synal, H. A.: Accelerator Mass Spectrometry of ^{129}I towards its lower limits, Nucl. Instrum. Meth. B, 361, 445–449, https://doi.org/10.1016/j.nimb.2015.01.061, 2015.

von Appen, W.-J., Koszalka, I. M., Pickart, R. S., Haine, T. W. N., Mastropole, D., Magaldi, M. G., Valdimarsson, H., Girton, J., Jochumsen, K., and Krahmann, G.: The East Greenland Spill Jet as an important component of the Atlantic Meridional Overturning Circulation, Deep-Sea Res. Pt. I, 92, 75–84, 2014.

Wagner, M. J. M., Dittrich-Hannen, B., Synal, H. A., Suter, M., and Schotterer, U.: Increase of ^{129}I in the environment, Nucl. Instrum. Meth. B, 113, 490–494, 1996.

Winkler, S. R., Steier, P., and Carilli, J.: Bomb fall-out ^{236}U as a global oceanic tracer using an annually resolved coral core, Earth Planet. Sc. Lett., 359–360, 124–130, https://doi.org/10.1016/j.epsl.2012.10.004, 2012.

Xu, X., Schmitz Jr., W. J., Hurlburt, H. E., Hogan, P. J., and Chassignet, E. P.: Transport of Nordic Seas overflow water into and within the Irminger Sea?: An eddy – resolving simulation and observations, J. Geophys. Res., 115, C12048, https://doi.org/10.1029/2010JC006351, 2010.

Xu, X., Bower A., Furey, H., and Chassignet, E.-P.: Variability of the Icelans-Scotland Overflow Water Transport through the Charlie-Gibbs Fracture Zone: results from an eddying simulation and observations, J. Geophys. Res.-Oceans, 123, https://doi.org/10.1029/2018JC013895, 2018.

Zou, S., Lozier, S., Zenk, W., Bower, A., and Johns, W.: Observed and modeled pathways of the Iceland Scotland Over flow Water in the eastern North Atlantic, Prog. Oceanogr., 159, 211–222, https://doi.org/10.1016/j.pocean.2017.10.003, 2017.

Zunino, P., Lherminier, P., Mercier, H., Daniault, N., García-Ibánez, M. I., and Pérez, F. F.: The GEOVIDE cruise in May–June 2014 reveals an intense Meridional Overturning Circulation over a cold and fresh subpolar North Atlantic, Biogeosciences, 14, 5323–5342, https://doi.org/10.5194/bg-14-5323-2017, 2017.